SLAC-PUB-2865
LBL-13835
December 1981
(T/E)

EXPERIMENTAL UPPER LIMITS ON BRANCHING FRACTIONS FOR UNEXPECTED DECAY MODES OF THE TAU LEPTON*

K.G.Hayes,† M.L.Perl, M.S.Alam,** A.M.Boyarski, M.Breidenbach, D.L.Burke, J.Dorenbosch,† J.M.Dorfan, G.J.Feldman, M.E.B.Franklin, G.Hanson, T.Himel,‡ D.G.Hitlin,‡ R.J.Hollebeek, W.R.Innes, J.A.Jaros, P.Jenni,† R.R.Larsen, V.Lüth, B.Richter, A.Roussarie,¶ D.L.Scharre, R.H.Schindler,† R.F.Schwitters,§ J.L.Siegrist, H.Taureg,† M.Tonutti,‖ R.A.Vidal, J.M.Weiss, and H.Zaccone¶
Stanford Linear Accelerator Center
Stanford University, Stanford, California 94305

G.S.Abrams, C.A.Blocker, A.Blondel, W.C.Carithers, W.Chinowsky, M.W.Coles,‡‡ S.Cooper,‡‡ W.E.Dieterle, J.B.Dillon, M.W.Eaton, G.Gidal, G.Goldhaber, A.D.Johnson, J.A.Kadyk, A.J.Lankford, M.Levi,§ R.E.Millikan, M.E.Nelson, C.Y.Pang, J.F.Patrick, J.Strait, G.H.Trilling, E.N.Vella, and I.Videau
Lawrence Berkeley Laboratory and Department of Physics
University of California, Berkeley, California 94720

ABSTRACT

Searches for 12 neutrinoless decay modes of the tau which violate lepton number conservation have been made using the reaction $e^+e^- \to \tau^+\tau^-$. No evidence for lepton number violation is observed, and we have set upper limits (90% C.L.) on the branching ratio for each decay mode. The branching ratio limits on the radiative decays $\tau \to \mu\gamma$ and $\tau \to e\gamma$ are .055% and .064% respectively. For the charged lepton decays $\tau \to eee$, $\tau \to e\mu\mu$, $\tau \to \mu ee$, and $\tau \to \mu\mu\mu$, the branching ratio limits are .040%, .033%, .044%, and .049% respectively. Upper limits on the branching ratios for the following charged lepton+ neutral hadron decays are: $\tau \to e\rho^o$ (.037%), $\tau \to \mu\rho^o$ (0.044%), $\tau \to eK^o$ (.13%), $\tau \to \mu K^o$ (.10%), $\tau \to e\pi^o$ (.21%), and $\tau \to \mu\pi^o$ (.082%). We also use these data to search for the pair production in e^+e^- annihilation of some unconventional particles with masses less than about 3 GeV/c^2.

---

*Work supported by the Department of Energy under contract numbers DE-AC03-76SF00515 and W-7405-ENG-48.

**Present address: Vanderbilt University, Nashville, Tennessee 37235
†Present address: CERN, Geneva, Switzerland
‡Present address: California Institute of Technology, Pasadena, California 91125
§Present address: Harvard University, Cambridge, Massachusetts 02138
‖Present address: Universität Bönn, D-53 Bönn, Federal Republic of Germany
¶Present address: Centre d'Etudes Nucléaires de Saclay, F-91190 Gif-sur-Yvette, France
‡‡Present address: DESY, Hamburg, Germany

(Submitted to Physical Review)

1. INTRODUCTION

This paper describes a search for decay modes of the tau lepton (τ) which do not contain the tau neutrino (ν_τ). We did not find these modes; and we report upper limits on the branching fractions. The absence of such modes is consistent with our current model of the τ, which states that the τ^- and ν_τ have a unique conserved lepton number.

This search was carried out using the τ production reaction

$$e^+ + e^- \rightarrow \tau^+ + \tau^- \qquad (1)$$

at the SPEAR electron-positron colliding beams facility of the Stanford Linear Accelerator Center. The Mark II Magnetic Detector was used to acquire about 17,000 nb^{-1} of data in the center-of-mass energy range of $3.85 \leq E_{c.m.} \leq 6.85$ GeV.

We also use these data to search for the pair production of unconventional particles with masses less than about 3 GeV/c^2 which might be produced in e^+e^- annihilation. For example, we searched for an excited electron, e^*, with the decay mode $e^* \rightarrow e + \gamma$.

The theory associated with the nature and decay properties of the τ has been discussed in detail in many papers[1-4]; and there is no need to review that material here. This is particularly true because the τ behaves so simply. All recent, published, experimental studies of the production and decay properties of the τ agree[1,2] with the following model:

a. The τ is a spin 1/2, point particle obeying the Dirac equation.

b. The τ^- and its associated neutrino, ν_τ, have a unique, conserved, lepton number.

c. The τ decays only through the weak interaction with V-A coupling.

According to this model all decays of the τ have the form

$$\tau^- \to \nu_\tau + a + b + \ldots . \quad , \tag{2}$$

and decay modes which do not contain the ν_τ violate this model.

We have searched for three types of model-violating decay modes:

Radiative modes: (3)

$$\tau^- \to e^- + \gamma$$

$$\tau^- \to \mu^- + \gamma$$

Three lepton modes: (4)

$$\tau^- \to e^- + e^+ + e^-$$

$$\tau^- \to \mu^- + e^+ + e^-$$

$$\tau^- \to e^- + \mu^+ + \mu^-$$

$$\tau^- \to \mu^- + \mu^+ + \mu^-$$

Neutral hadron decay modes: (5)

$$\tau^- \to e^- + \pi^o$$

$$\tau^- \to \mu^- + \pi^o$$

$$\tau^- \to e^- + K^o$$

$$\tau^- \to \mu^- + K^o$$

$$\tau^- \to e^- + \rho^o$$

$$\tau^- \to \mu^- + \rho^o$$

Note that for brevity, when we describe a decay mode using the τ^- we also include the charge conjugate decay mode of the τ^+. Thus a search for $\tau^- \to e^- + \gamma$ includes a search for $\tau^+ \to e^+ + \gamma$.

This paper is limited to a presentation of our experimental results. We shall not attempt to discuss the detailed limitations these results put on the various possible modifications of the conventional theory of the τ. Some of these limitations have been described by K. G. Hayes[5].

The plan of this paper is as follows. The apparatus, data acquisition and general search method are described in Secs. 2 and 3. Sections 4, 5, and 6 present the search method and results for the types of decay modes listed in Eqs. 3, 4, and 5 respectively. Finally, in Sec. 7 we describe the search for unconventional particles using this data, and we summarize the null results.

2. APPARATUS AND DATA ACQUISITION

Figures 1 and 2 show cross sectional and isometric views of the Mark II Magnetic Detector. As a particle leaves the interaction region it passes thru the beam pipe, and then through a set of cylindrical scintillation counters, called the pipe counters. The particle then enters the cylindrical drift chamber.

This drift chamber[6], with inner and outer radii of 0.41m and 1.45m respectively, is immersed in a longitudinal, solenoidal, 0.4T magnetic field. Charged particles are detected in over 80% of the solid angle. The chamber has 16 layers; six are parallel to the beam axis, and the other ten are rotated by about $\pm 3^{o}$ to determine the momentum component along the beam axis. The average momentum resolution is

$$\Delta p/p = .01\sqrt{(1.5)^2 + p^2} \qquad (6)$$

where the constant term represents the effects of multiple coulomb scattering, and the momentum dependent term accounts for the 200 micron single cell resolution. Here p is the momentum in GeV/c.

The time of flight scintillation counters are located between the drift chamber's outer cover and the solenoid coil, at a 1.5 meter radius from the beam axis. The scintillator is viewed at both ends to give a time resolution of 300 picoseconds. This allows separation of electrons from pions below 300 MeV/c, kaons from pions below 1.3 GeV/c, and protons from pions below 2.0 Gev/c.

The lead and liquid argon electromagnetic shower detector lies just outside the magnet coil. Eight modules completely surround the detector

in azimuth and cover 60% of the total solid angle. The detector consists of 37, 2mm thick, lead plates separated by 3mm gaps filled with liquid argon. The total number of radiation lengths in the detector is 14. The lead plates are alternately continuous ground planes and ionization signal collecting high voltage planes. The latter are divided into strips which provide spatial information. The electromagnetic energy resolution is

$$\Delta E/E = .13/\sqrt{E(GeV)} \qquad (7)$$

Electrons are separated from hadrons and muons using the properties of the electromagnetic shower. The principal properties used are the ratio of the shower energy to the momentum of the particle, and the ratio of the energies deposited in the front and back of the module. The actual algorithm is quite complicated and is discussed in Refs. 5 and 7. Table I gives the probability of misidentifying a $\pi^{\pm}$ as an $e^{\pm}$ using the shower detector and time-of-flight counter information.

The photon detection efficiency, Fig. 3, was measured using constrained fits to the processes $\psi \to \pi^+\pi^-\pi^o$ and $\psi \to 2\pi^+2\pi^-\pi^o$. Upward fluctuations in the electronic noise can cause false photons to be found by the photon detection software. The threshold in the efficiency is caused by the cuts required to keep the spurious photon rate acceptable.

The muon identification system, which lies outside the liquid argon shower detectors, consists of several layers of thick steel plates and proportional tubes, Figs. 1 and 2. Before a particle can reach the first plate, it must traverse inner detector material, the

magnet coil and the shower detector, equivalent to 20 cm of iron. The steel absorbing plates are 23 cm thick in the first two layers and 30 cm thick in the third layer of the top wall. The first layer is located approximately 3 meters from the interaction region, and subtends 51% of the solid angle, while the second layer is approximately of equal area and covers 90% of the solid angle subtended by the first. The top wall's third layer subtends 9% of the total solid angle. The momentum of a muon must exceed about 700 MeV/c to penetrate the first layer.

Behind each absorbing plate there is a plane of proportional tubes which run the full width of the wall and which measure one of the two orthogonal coordinates. The tubes are oriented so that the second and third layers measure the coordinate orthogonal to that measured by the first. The 1672 tubes used in the system are actually built in the form of eight-tube modules made of extruded aluminum, Fig. 4. The ability of this system to separate hadrons from muons is discussed in Ref. 5. An illustration of that ability is given in Fig. 5.

Data was acquired using a two level system[8] composed of a fast (500 nsec.) primary trigger whose output sets off a more sophisticated but slower (30 μsec.) secondary trigger. The primary trigger demands the coincidence of a beam crossing signal from a pickup electrode with the pipe counter, and hits in at least 4 of 9 selected drift chamber layers. The pipe counter limits the cosmic ray background to tracks which pass within 12 cm of the beam axis. The loose requirement on the drift chamber data results in near perfect efficiency for tracks which pass through all of the drift chamber layers.

The secondary trigger is an electronic track finder and track counter. It works by rotating crescent shaped masks axially around the drift chamber and defining tracks if a minimum number of layers have hits within the mask boundaries. Twenty-four masks are used, allowing tracks of different momenta and charge to be recognized. The criterion used for most of the experiment was at least 1 track with 4 out of 6 axial layers hit, and 1 track with at least 3 hits in the five innermost layers. This resulted in a trigger rate of a few hertz. The combination drift chamber and trigger logic system worked so well that the trigger efficiency for event topologies used in this analysis (that is, tracks which enter the shower detector or muon system solid angle) is nearly 100%.

The data collected during the fall of 1978 and spring 1979, and listed in Table II, was used in this analysis. We give for each energy interval the integrated luminosity and the number of produced tau pairs; the latter being calculated from the luminosity and the tau cross section.[1] The systematic error in the luminosity is estimated to be 6%.

3. GENERAL SEARCH METHOD

We searched for unexpected decay modes by requiring that one of the τ's in

$$e^+ + e^- \rightarrow \tau^+ + \tau^- \qquad (8a)$$

decay into one of the known, single-charged prong, decay modes. The single-charged prong, decay modes are mainly:

$$\tau^+ \to e^+ + \nu_e + \bar{\nu}_\tau$$

or

$$\tau^+ \to \mu^+ + \nu_\mu + \bar{\nu}_\tau \qquad (8b)$$

or

$$\tau^+ \to \pi^+ + \bar{\nu}_\tau$$

or

$$\tau^+ \to \rho^+ + \bar{\nu}_\tau \to \pi^+ + \gamma + \gamma + \bar{\nu}_\tau$$

The other τ could then decay unconventionally; such as

$$\tau^- \to e^- + \gamma$$

or

$$\tau^- \to \mu^- + \gamma$$

or

$$\tau^- \to e^- + e^+ + e^- \qquad (8c)$$

or

$$\tau^- \to e^- + \rho^o \to e^- + \pi^+ + \pi^-$$

and so forth. Of course, the roles of the τ^+ and τ^- could be reversed.

This basic signature in a perfect detector lends to events with 2 or 4 charged particles with total charge zero, and with up to two photons. To satisfy this signature in our detector we selected events with the following properties:

a) 2, 3, or 4 charged tracks;

b) total charge = 0 for 2 or 4 track events;

c) total charge = ± 1 for 3 track events;

d) any number of photons; and

e) the 2 charged track events have an acoplanarity angle[9] greater than 5^{o}.

The sample containing a total of three charged tracks allowed us to use events in which the three charged particles in an unconventional decay such as $e^- + e^+ + e^-$ were detected, but the track from the conventional decay was not detected. The acoplanarity requirement eliminates background from $e^+e^- \to e^+e^-$, $\mu^+\mu^-$.

4. SEARCH FOR THE RADIATIVE DECAY MODES $\tau^- \to e^-\gamma$, $\mu^-\gamma$

In this search we use two track, total charge zero events with one or more photons

$$e^+ + e^- \to \ell^\pm + x^\mp + \text{1-or-more } \gamma\text{'s} \qquad (9)$$

Here ℓ means e or μ; x means e, μ, or hadron.

To reduce the contamination from beam-pipe or beam-gas events, the reconstructed vertex of the two charged prongs must lie within a cylinder 16 cm long with a 4 cm radius centered around the interaction region. To eliminate mis-measured tracks, the vertex finding algorithm must use both tracks, and the chi-square from the vertex fit must be less than 100. A minimum momentum cut of 100 MeV/c is applied to the charged tracks to insure a well defined cutoff in the detector's response to low momentum tracks.

The invariant mass, m, of the photon-lepton system in Eq. 9 is

$$m = \left[m_\ell^2 + 2E_\gamma \, (E_\ell - p_\ell \cos\theta)\right]^{\frac{1}{2}} \qquad (10)$$

Here E_ℓ and p_ℓ are the energy and momentum of the lepton, E_γ is the energy of the photon, and θ is the angle between the photon and lepton. The resolution in this measurement is dominated by the relatively poor photon energy resolution. Since the tau is pair produced, the sum of the energies of its decay products equals the beam energy, and this constraint can be used to improve the resolution of the invariant mass measurement.

The proper realization of the beam constraint adjusts both the measured photon and lepton energies depending on their relative measurement errors, but in practice is nearly identical to the simple replacement of the photon energy with

$$E_{\gamma,\text{used}} = E_{\text{beam}} - E_\ell \qquad (11)$$

Figure 6 shows the μ-γ mass resolution as a function of $x = E_{\ell}/E_{beam}$ for three beam energies. If the correct constraint procedure is applied, the resolution levels off as x approaches 1 at a value reflecting the photon energy resolution, but it is so poor that this kinematical region is useless. Consequently we require

$$x \leq .77 \tag{12}$$

In the allowed x region, the error in the predicted photon energy is small relative to the error in the photon energy measurement. Therefore, a cut on the chi-square of the 1-constraint fit is equivalent to a cut on the photon energy resolution variable

$$D = [E_{\gamma,used} - E_{\gamma}]/E_{\gamma,used}$$

This variable is normally distributed with a sigma of $.13/\sqrt{E_{\gamma,used}(GeV)}$ according to a Monte Carlo study. Hence

$$Z = D\sqrt{E_{\gamma,used}}$$

is normally distributed with a sigma of .13 $GeV^{\frac{1}{2}}$. We eliminate events with large $[E_{\gamma,used} - E_{\gamma}]$ by requiring

$$|Z| \leq .20 \text{ GeV}^{\frac{1}{2}} \tag{13}$$

Figure 7 shows the mass spectra using the entire data sample with the restrictions of Eqs. 12 and 13. Recall that we have also required that the acoplanarity angle be greater than 5^{o}.

These spectra contain background events from conventional electromagnetic reactions such as

$$
\begin{aligned}
&e^+ + e^- \to e^+ + e^- + \gamma \\
&e^+ + e^- \to e^+ + e^- + \gamma + \gamma \\
&e^+ + e^- \to \mu^+ + \mu^- + \gamma \\
&e^+ + e^- \to \mu^+ + \mu^- + \gamma + \gamma
\end{aligned}
\qquad (14)
$$

We reduce these backgrounds by a set of constraints discussed in detail in Ref. 5. We shall list these constraints here:

a) The event must not conserve three-momentum using just the ℓ, x, and γ's in Eq. 9.

b) The event must not be consistent with having an undetected photon along the beam direction of greater than 300 MeV energy.

These two constraints remove 65% of the μ-γ candidates and 45% of the e-γ candidates. A small additional fraction of candidates are removed by:

c) The cosine of the angle between the photon and the ℓ-x plane must be less than .998.

d) The cosine of the angle between the photon and either the ℓ or the x must be less than .986.

e) The γ must not reconstruct with another γ in the event to the π^o mass.

Two additional restrictions are made on the e-γ candidates because of the larger contamination from the reactions in Eq. 14:

f) The acoplanarity angle[9] must be greater than 28^o.

g) The $x^{\pm}$ in Eq. 9 cannot be an identified $e^{\pm}$.

The effect of constraints a.-g. on the acceptance is shown in Fig. 8. We see that the e-γ acceptance is reduced more than the μ-γ acceptance because of restrictions f. and g. The acceptance is calculated using a Monte Carlo method.

With the addition of the cuts discussed above, we obtain the μ-γ invariant mass spectrum shown in Fig. 9b. The spectrum in the region near the tau mass is shown with an expanded scale in Fig. 10b along with the resolution function obtained with the Monte Carlo.

There is no evidence for the $\mu+\gamma$ radiative decay of the tau. Using the measured luminosity and calculated acceptance, we can determine a 90% confidence level upper limit to the branching fraction

$$B \leq \lambda(N_{obs}) / \left[2 \sum_{E} \sigma(E) L(E) A(E)\right]$$

Here $\lambda(N)$ is the average value for a Poisson distribution such that there is a 90% probability that N_{obs} comes from a distribution with that average value or smaller. Here N_{obs} is the number of events observed within the mass acceptance region; σ is the $e^+e^- \rightarrow \tau^+\tau^-$ cross section; L is the luminosity; A is the acceptance; and E is the center of mass energy. The mean acceptance is 7.3%, averaged over the center of mass energy range with a weight function proportional to the number of produced tau pairs. Given that the data sample contains 96,000 produced tau leptons, the single event which lies within the 68 MeV/c^2 wide region used to define the acceptance determines the 90% confidence level on the branching ratio of the radiative decay $\tau \rightarrow \mu+\gamma$ to be .055%.

The e-γ mass spectrum is shown in Figs. 9a and 10a. There is no evidence for the e+γ radiative decay of the τ. The one event in Fig. 10a within the 68 MeV/c^2 acceptance interval leads to a 90% confidence level upper limit on the branching fraction for the decay $\tau \to e+\gamma$ of .064%.

In looking at Fig. 10, one notices quickly the collection of mass pairs in both eγ and $\mu\gamma$ at about 1730 MeV/c^2. The immediate question is, "Have we made an error in the mass scale of about 50 MeV/c^2 so that these mass pairs are from the eγ or $\mu\gamma$ decay of the τ?" We have examined this possibility by studying the possible systematic errors in the three quantities which determine the invariant mass, the beam energy E_{beam}, the lepton energy E_ℓ, and the angle between the lepton and photon θ. Recall that we use the beam constrained invariant mass so that the relatively poorly measured photon energy has little effect. As indicated by Eq. 11 we essentially use

$$m = \left[m_\ell^2 + 2(E_{beam} - E_\ell)\ (E_\ell - p_\ell \cos\ \theta) \right]^{\frac{1}{2}} \qquad (15)$$

The center of a beam constrained invariant mass resolution function depends upon the two very well measured quantities E_{beam} and θ, Eq. 15. Because of the way E_ℓ enters Eq. 15 and since E_ℓ has a flat spectrum for two-body decays, errors in E_ℓ broaden the resolution function, but do not shift the center appreciably. Hence any shift in the mass scale must come from systematic errors in E_b and θ. We have estimated these systematic errors and our upper limit on a mass scale shift is 12 MeV/c. Hence the eγ and $\mu\gamma$ pairs in the vicinity of 1730 MeV/c^2 in Fig. 10 do not come from decays of the τ. We return to these pairs in Sec. 7B.

4. SEARCH FOR THE THREE LEPTON DECAY MODES $\tau \to e^-e^+e^-, e^-\mu^+\mu^-, \mu^-e^+e^-, \mu^-\mu^+\mu^-$

About 70% of tau decays have one charged particle in the decay products. Therefore, in the search for the three charged lepton decays of the tau, we use all 3 and 4 charged prong events which have a total charge between -1 and 1, and which have one or more tracks identified as an electron or muon. No restrictions are placed on the number of neutral particles in the event. At least 3 of the charged tracks must form a vertex located within a cylinder 16 cm long and 4 cm in radius centered about the interaction region. To insure a well-defined momentum cutoff, all tracks used in any invariant mass calculation must have a momentum larger than 100 MeV/c and must originate in the event vertex.

The MARK II's acceptance to detect and identify all 3 leptons from any of the four tau decays listed in Eq.4 is small and decreases as the number of muons in the decay increases. Thus, we are forced to also consider 3 charged track combinations where only one or two tracks are identified as leptons. The background from random combinations increases with the number of unidentified tracks. Therefore, the contribution to each of the 4 decays from combinations where 1, 2 or 3 leptons are identified, are accumulated separately so that those with the worst background can be discarded. For example, contributions to the invariant mass distribution for the decay $\tau \to e\mu^+\mu^-$ can be from any of the following lepton combinations:

$$exx, \quad \mu xx, \quad e\mu x, \quad x\mu\mu, \quad e\mu\mu \tag{16}$$

where x represents a particle which was not identified as a lepton. Note that the electric charges of the particles are relevant. The combination exx can contribute to the decay only if x_1 and x_2 have opposite charges. If in the combination μxx, both x_1 and x_2 have the opposite charge from the muon, we will consider both cases, where either x_1 or x_2 is assigned the electron mass, and use only the combination which has the best chi-square for the beam constrained fit.

Given the measured 3 momentum and a mass hypothesis for each charged track, the invariant mass of the three charged track combination is

$$m = \left[\left(\sum_i E_i\right)^2 - \left(\sum_i P_i\right)^2\right]^{\frac{1}{2}} \tag{17}$$

The resolution in this measurement depends on the center of mass energy and the number of electrons in the decay. For the 3 muon decay, the resolution is typically 20 to 30 MeV/c^2, but it is several times worse for the eee decay. This can be improved by a factor of 2 to 3 if the fact that the tau is produced with the beam energy is used to correct the measured track momenta. We define

$$\Delta E = E_{beam} - \sum_i E_i \tag{18}$$

and

$$Z = \sum_i E_i / E_{beam} \tag{19}$$

Obviously we want ΔE to be small and so we set the following requirements on Z.

$$A < Z < 1.03 \tag{20}$$

$$A(\mu\mu\mu) = .97, \quad A(e\mu\mu) = .96 = A(\mu ee) \quad A(eee) = .95$$

All candidates which pass this Z requirement are then subject to a fit which varies the three particle energies so as to satisfy the beam energy constraint. These energies and the measured angles are then used to calculate the three-particle invariant mass M_3.

There are many different sources which contribute background to this search, for example, electromagnetic events, hadronic events where pions are misidentified or decay to muons, converted photons in hadronic events, semi-leptonic decays of charmed particles, and tau events. Therefore we use the following set of restrictions, which are discussed fully in Ref. 5.

a) An event must not contain an electron pair from a converted photon.

b) The average of the cosine of the coplanarity angle between a track and all other tracks in the event must be larger than -.970 for all tracks. This eliminates most Bhabha scattering events in which one of the electrons is accompanied by an electron pair.

The acceptances for the various modes range from .01 to .20; Fig. 11 shows some examples.

The distributions for the invariant mass M_3, for 3-electron combinations with 1, 2, or 3 identified electrons are shown in Fig. 12.

There is no evidence in the plot for the decay $\tau \to eee$. Figs. 13-15 show the equivalent plot for the other three decays: $\tau \to \mu ee$, $\tau \to e\mu\mu$, and $\tau \to \mu\mu\mu$. Again, no evidence can be seen for the decay of the tau to any three charged lepton combination.

Table III is a summary of the data for each of the 4 decays in this search. In this table we list, subdivided according to the category of identified leptons, the average acceptance for each decay, the number of detected events within the 40 MeV/c^2 region used to define the acceptance, and the 90% confidence level upper limit on the branching ratio. Within any single decay, the results from different sets of identified lepton categories are statistically independent as different particle combinations contribute to each category. By adding the categories with the least background together, the overall limit on the branching ratios can be improved. Table IV summarizes the best limits obtainable in this way.

6. SEARCH FOR DECAY OF THE τ TO A CHARGED LEPTON PLUS NEUTRAL HADRON

In this section we describe the search for the decay modes

$$\tau^- \to e^- + \rho^o \ , \ \tau^- \to \mu^- + \rho^o \tag{21}$$

$$\tau^- \to e^- + K^o \ , \ \tau^- \to \mu^- + K^o \tag{22}$$

$$\tau^- \to e^- + \pi^o \ , \ \tau^- \to \mu^- + \pi^o \tag{23}$$

Although these are two body decays, the hadrons are short-lived and can be measured only by detecting their decay products. The ρ^o is reconstructed from its $\pi^+\pi^-$ decay. As its large width allows only a loose mass cut to be made, the analysis is very similar to that of the three

charged lepton decays discussed in Sec. 5. The K^o is reconstructed from the $\pi^+\pi^-$ decay mode of its short-lived component. The fact that the K^o can travel an appreciable distance from the interaction region before decaying, and the kinematic constraint provided by its narrow width requires a more detailed analysis to be made but results in an improved signal to background ratio relative to the rho-lepton decay. Photons detected in the liquid argon shower detector are used to reconstruct the π^o. The shower counter detection efficiency and limited solid angle restrict the acceptance, resulting in a reduced sensitivity for the $\ell^\pm + \pi^o$ decay mode search.

The data sample, containing 48000 produced tau pairs, is the same used in the previous analyses. The event topology used in the $\ell^\pm + \rho^o$ and $\ell^\pm + K^o$ search is the same as that used in the three charged lepton decay search (except for one vertex cut in the K^o analysis), while the topology used in the $\ell^\pm + \pi^o$ search is the same as that used in the $\ell^\pm + \gamma$ search except that we require at least two photons to be detected in the event. Other similarities exist between this analysis and the previous ones, and we shall make many references to material previously presented.

The remainder of this section is divided into three parts. First we will discuss the search for the $\ell^\pm + \rho^o$ decay of the tau, followed by $\ell^\pm + K^o$ and $\ell^\pm + \pi^o$ searches.

6.A. Search for $\ell^{\pm} + \rho^{o}$:

The search for $\ell^{\pm} + \rho^{o}$ is very similar to the three charged lepton analysis discussed in Sec. 5 for the μxx and exx identification categories. There are only three differences:

a) The two x tracks are assumed to be pions and must have opposite charge.

b) To reduce the background a tighter cut is applied on the measured total energy of the three tracks. Defining

$$Z = (E_{\ell} + E_{\pi^+} + E_{\pi^-})/E_{beam} \tag{24}$$

and

$$y = (E_{c.m.} - 4.0)\ \text{GeV} \tag{25}$$

we require

$$\begin{aligned} \mu+\rho: &\quad .975(1-.0038y) < Z < 1.025(1+.0038y) \\ e+\rho: &\quad .975(1-.0038y) < Z < 1.020(1+.0038y) \end{aligned} \tag{26}$$

As the resolution in Z changes with the beam energy, the cut is now made to vary with the total energy. (In the analysis of the three lepton decay modes, the resolution in Z also changes with energy, but the background was smaller there and we could use a simpler, fixed Z cut.)

c) The invariant mass of the two pions must be consistent with the ρ^{o} mass. In Fig. 16 we plot the measured 2 pion invariant mass distribution for all $\mu-(\pi^+\pi^-)$ candidate events passing the total energy (Z) cut compared to the Breit-Wigner distribution expected for the rho. A small rho signal is seen, and to maximize the signal to background ratio, the $\pi^+\pi^-$ invariant mass is required to be within 100 MeV/c^2 of the rho mass.

The beam-constrained $\ell^{\pm} + \rho^{o}$ mass distributions obtained after applying the above cuts are shown in Figs. 17 and 18 for the μ-ρ and e-ρ candidates. We see no evidence for the decays $\tau \to \mu + \rho$ or $\tau \to e + \rho$.

The acceptance using those events within 20 MeV/c^2 of the tau mass is 5.5% for the $\tau \to \mu - \rho$ and 6.5% for the $\tau \to e - \rho$ decay. Given that no μ-ρ events are detected within the acceptance window, the 90% confidence level upper limit on the branching ratio for the decay $\tau \to \mu + \rho$ is .044%. There are also no e-ρ events detected within the acceptance window. The 90% C.L. upper limit on the branching fraction for the decay $\tau \to e + \rho$ is .037%.

6.B. Search for $\ell^{\pm} + K^{o}$:

The search for $\ell^{\pm} + K^{o}$ is somewhat more involved than the search for $\ell^{\pm} + \rho^{o}$. Since we only use the decay mode $K^{o}_{s} \to \pi^{+} + \pi^{-}$, the net acceptance will be reduced by a factor of .34. However, the fact that the kaon decay vertex is most often located away from the primary vertex can be used to significantly reduce the background. But we can no longer demand that the two pion tracks originate in the primary vertex. All the other vertex, topological, and background removing cuts used in the 3 charged lepton tau decay search are retained.

The K^{o} reconstruction algorithm is straightforward and yields a relatively clean kaon sample. We exploit the fact that in the uniform magnetic field of the Mark II, the charged particle

trajectories projected in the xy plane are circles. The decay vertex is located at one of the two points where the circles intersect, and the invariant mass of the two tracks, calculated with the momenta measured at the decay vertex (not the point of closest approach to the interaction region) is--within errors-- the K^o mass. The algorithm is described in detail in Ref. 5. Figure 19 shows the dipion invariant mass distribution from a sample of multiprong as well as two-prong events. The K^o mass resolution is $\sigma \approx 6$ MeV/c^2. Only those pairs with a mass within 18 MeV/c^2 of the kaon mass are retained.

We now address the question of the kinematic constraints which exist for this decay mode. We use Z and y as defined in Eqs. 24 and 25. The beam energy constraint applies as before although the Z restriction must be made looser because the momentum resolution is degraded for tracks which do not originate near the interaction region. We use

$$\begin{aligned} \mu+K^o: \quad & .960(1-.0077y) < Z < 1.040(1+.0077y) \\ e+K^o: \quad & .950(1-.0077y) < Z < 1.040(1+.0077y) \end{aligned} \tag{27}$$

These cuts were determined using the Monte-Carlo simulation program and are looser than the $\ell^{\pm} + \rho^o$ cuts both because the resolution is poorer, and because the background is much reduced due to the K^o requirement.

For those candidates which pass the Z cut, we apply the beam constraint technique to improve the $\ell^{\pm} + K^o$ mass resolution. This yields a mass resolution $\sigma \approx 8.7$ MeV/c^2.

The $\mu+K^o$ and $e+K^o$ mass distributions are shown in Fig. 20. The distributions contain no evidence for these decay modes of the tau. The acceptance is 2.4% for the $\mu+K^o$ decay and 3.1% for the $e+K^o$ decay of the tau. Given that no $\mu+K^o$ events are observed which have an invariant mass within 20 MeV/c^2 of the tau mass, we can set a 90% confidence level upper limit on the branching fraction for the decay $\tau\to\mu+K^o$ of .10%. The single $e+K^o$ event observed in the 40 MeV/c^2 acceptance window determines the 90% C.L. upper limit on the branching fraction for the decay $\tau\to e+K^o$ of .13%.

6.C. Search for $\ell + \pi^o$:

The final charged lepton+neutral hadron tau decays we shall discuss are the $\tau\to\mu+\pi^o$ and $\tau\to e+\pi^o$ decays. This analysis is in many ways similar to that of the search for the $\ell+\gamma$ decays discussed in Sec. 4. A subset of the events used in that analysis are used here : two oppositely-charged, acoplanar tracks which originate in the interaction region, one or more of which is identified as a lepton, with 2 or more photons detected in the liquid argon shower detector. Therefore there are the same sources of background. The restrictions discussed in Sec. 4 to eliminate events of purely electromagnetic origin are also used in this analysis as they have a negligible effect on the acceptance, less than 2%, but reduce the background significantly. Because the $\ell+\pi^o$ mass resolution is dominated by the photon energy resolution, the beam constraint technique yields nearly the same mass

resolution as existed in the radiative decay search, and the inclusion of the pion mass constraint improves this somewhat. The acceptance is significantly smaller, however, as the two photons from the decay must be detected, and the sensitivity of this search is correspondingly reduced.

The π^o reconstruction algorithm is simple: all photon pairs whose invariant mass is consistent with the neutral pion mass are called π^o's. No attempt is made to resolve the ambiguity if a photon is used in more than one π^o. The π^o mass resolution, Fig. 21, depends upon the π^o energy and the π^o decay asymmetry parameter

$$a = .5 - \frac{|E_1 - E_2|}{2(E_1 + E_2)} \tag{28}$$

Here E_1 and E_2 are the energies of the γ's.

Two major cuts are used to decide whether a given photon pair is to be called a π^o. The pair is required to have an invariant mass between 50 and 250 MeV/c^2. Pairs which survive this cut are subject to a 1-C fit to the π^o mass in which all the photon parameters are varied, and those which have an χ^2 less than 5 are called π^o's. These cuts are loose and maximize the π^o detection efficiency at the expense of a large background.

Having reconstructed the π^o's, the invariant mass is calculated for all $\ell^\pm + \pi^o$ combinations which have a total energy consistent with the beam energy. As the resolution in $E_{tot} = E_\ell + E_{\pi^o}$ varies with

the lepton and pion energy, a cut is applied to the normalized variable

$$Y = (E_{tot} - E_{beam})/\sigma(E_{tot}) \qquad (29)$$

where $\sigma(E_{tot})$ is the sigma for E_{tot}. Y^2 is equal to the χ^2 for the 1-C fit constraining E_{tot} to the beam energy. Figure 22 shows the measured Y distribution for both the $e+\pi^o$ and $\mu+\pi^o$ candidates along with the expected distributions for $\ell+\pi^o$ tau decays calculated with the Monte Carlo simulation program. All combinations for which the magnitude of Y is greater than 2 are rejected.

The $\ell+\pi^o$ mass resolution varies with the asymmetry of the decay, and deteriorates rapidly as the lepton energy approaches the beam energy. Hence we reject events with $E_\ell/E_{beam} > .8$.

Figure 23 shows the constrained $\ell+\pi^o$ mass for all candidates passing the decay constraints. A large background is present which originates from several sources, and the following restrictions[5] are used to suppress it:

a) The π^o must not contain a photon coming from an electron bremsstrahlung.

b) Each photon in the π^o must have greater than 200 MeV energy. This removes background due to false photons created by noise in the shower detector electronics.

c) The a of the π^o, Eq. 28, must be greater than .15. This reduces the background in π^o's of moderate to high energy due to the incorrect but statistically preferred pairing of one low energy and one high energy background photon.

d) The acoplanarity angle[9] must be greater than 12°.

e) The invariant mass of the π^{o} and of the non-ℓ charged particle must not lie in the ρ^{o} mass region of 650 to 950 MeV/c^2. This eliminates background from tau pair decays which contain $\tau^{\pm}\rightarrow\rho^{\pm}+\nu$.

Figure 24 shows the $\ell+\pi^{o}$ mass distributions with these constraints. No evidence is seen for the $\mu+\pi^{o}$ decay of the tau. The acceptance is 2.9%. No events are detected within the 40 MeV/c^2 region which defines the acceptance. This determines the 90% confidence level upper limit to the branching fraction for $\tau\rightarrow\mu+\pi^{o}$ to be .082%.

Finally we turn to the search for $\tau\rightarrow e+\pi^{o}$. After application of all constraints discussed above, three events remain in the 40 MeV/c^2 wide bin encompassing the τ mass. The acceptance is 3.5%. The 90% confidence level upper limit on the branching fraction for for the decay $\tau\rightarrow e+\pi^{o}$ is .21%.

7. SEARCH FOR UNCONVENTIONAL PAIR PRODUCED PARTICLES

In the analyses described in Secs. 4-6, we did not require that the particle have the tau mass until the acceptance was calculated. Hence the mass spectra in Figs. 9, 12-15, 17, 20, and 23 apply to any pair produced particle, $x^{\pm}$, with the indicated decay mode. Since the spectra extend from less than 1 GeV/c^2 to above 3 GeV/c^2 these

figures summarize a general search for particles in this mass range produced via

$$e^+ + e^- \rightarrow x^+ + x^- \qquad (30)$$

The bin width in the figures is 25 or 40 MeV/c^2, and the σ of the expected mass resolution is 8 to 30 MeV/c^2. new particle would be indicated by a peak of substantial statistical significance with a width of up to several bins. We do not observe such a peak in any of these spectra.

A great deal of work is required to convert this qualitative observation to quantitative upper limits on the products of production cross sections and branching fractions. Monte Carlo methods must be used to calculate the acceptance and mass resolution at all masses of interest. Furthermore one must assume a knowledge of all the decay modes in order to calculate the probability of the x^+x^- pair fitting the basic event signature of Eq. 8.

We felt that it was worthwhile to carry out such calculations for the hypothetical particles called ortholeptons or excited leptons[10]. We studied two types. The μ^* has only one decay mode

$$\mu^{*\pm} \rightarrow \mu^{\pm} + \gamma \quad ; \qquad (31a)$$

and is produced via

$$e^+ + e^- \rightarrow \mu^{*+} + \mu^{*-} \qquad (31b)$$

We have not considered $e^+ + e^- \rightarrow \mu^{*\pm} + \mu^{\mp}$. Analogously we

considered

$$e^{*\pm} \rightarrow e^{\pm} + \gamma \tag{32a}$$

produced via

$$e^{+} + e^{-} \rightarrow e^{*+} + e^{*-} \tag{32b}$$

Pioneering searches for the e^* were carried out at the ADONE e^+e^- colliding beams facility[11].

7.A. Search for $\mu^* \rightarrow \mu + \gamma$

We assume

$$\sigma(ee \rightarrow \mu^*\mu^*) = R_{\mu^*} \frac{2\pi\alpha^2\beta(3-\beta^2)}{3E^2_{c.m.}} \tag{33}$$

where β is the lepton velocity in units of c and α is the fine structure constant. We use Fig. 9b to calculate upper limits on R_{μ^*}. Figures 25 and 26 show respectively the μ^* mass resolution and the acceptance for detecting the decay $\mu^* \rightarrow \mu + \gamma$. Figure 27 gives the number of $\mu^* \rightarrow \mu + \gamma$ which would have been detected if $R_{\mu^*} = 1$. For masses between .6 and 2.2 GeV/c^2 we would expect to detect approximately 8000 μ^*'s if they were produced with the point cross section and decayed with unit branching fraction to the $\mu+\gamma$ final state. For masses below .5 GeV/c^2, the decreasing acceptance limits this while above 2.6 GeV/c^2 only the high energy data contributes. The steep shoulder between 2.2 and 2.6 GeV/c^2 is a reflection of the threshold function in the cross section and the large fraction of data with $E_{c.m.} = 5.2$ GeV.

Using Figs. 9b and 27 we can determine an upper limit for the cross section suppression factor R_{μ^*}. In Table V we list, for various

mass intervals, 90% confidence limit upper limits on R_{μ^*}. These are worst case values obtained by dividing the 90% Poisson probability for the largest sum of three adjacent bins within the mass interval by the minimum expected number of detected events. Within these intervals there are certain regions where the limits are considerably better than the worst case values, but never better than .0004.

7.B. Search for $e^* \to e + \gamma$:

We determine upper limits on R_{e^*} for e^*'s produced via $e^+e^- \to e^{*+}e^{*-}$ in exactly the same way that upper limits on R_{μ^*} were set. Here

$$\sigma(ee \to e^*e^*) = R_{e^*} \frac{2\pi\alpha^2\beta(3-\beta^2)}{3E^2_{c.m.}} \qquad (34)$$

However the condition used to search for $\gamma \to e + \gamma$ in Sec. 4, that the track opposite to the $e + \gamma$ not be an electron, cannot be used. This leads to the $e+\gamma$ mass distribution shown in Fig. 28. The expected number of detected $e+\gamma$ events (shown as a function of the e^* mass in Fig. 29) is less than the μ^* case due to the tighter acoplanarity cut. Table VI lists the resulting 90% confidence level upper limits on R_{e^*} for various mass intervals.

Before concluding the paper we return to the question of whether significance should be attached to the existence in Fig. 10 of 5 $e\gamma$ mass pairs and 4 $\mu\gamma$ mass pairs in the vicinity of 1730 MeV/c^2. Figure 10 shows a small mass range of Fig. 9. In Fig. 9 there are 70 $\mu\gamma$ mass pairs and 72 $e\gamma$ mass pairs. Our first task is to calculate the probability that these 9 pairs occur in the vicinity of 1730 MeV/c^2 by chance.

These 9 mass pairs occupy a mass range of 16 MeV/c^2 which makes their appearance so striking. However as shown in Fig. 10 the width of the mass resolution curve at the τ mass is about 40 to 50 MeV/c^2. Since this width varies slowly with the mass, Fig. 25, we will have similar resolution curve widths at 1730 MeV/c^2.

We can calculate the probability of obtaining by chance this combination of 9 pairs in a 16 MeV/c^2 width, and we do so below. However, we believe that a larger width should be used to give such a calculation physical significance. We choose that larger width as being 30 or 40 MeV/c^2, since a reasonable fraction of the area of a resolution curve falls within that width. We define P(W,9,4) as the total probability of finding two peaks within a range of W MeV/c^2; eachpeak having at least 4 pairs, and the total being at least 9 pairs.

Assuming the backgrounds of Fig. 9 and Poisson statistics we find

$$P(16\ \text{MeV}/c^2,\ 9,4) = 0.0013$$
$$P(30\ \text{MeV}/c^2,\ 9,4) = 0.065 \qquad (35)$$
$$P(40\ \text{MeV}/c^2,\ 9,4) = 0.30$$

The coincidence of the peaks in Fig. 10 would still be apparent if each of the peaks had at least 3 pairs and the total was at least 9. Therefore we also consider the larger probabilities

$$P(16\ \text{MeV}/c^2,\ 9,3) = 0.0021$$
$$P(30\ \text{MeV}/c^2,\ 9,3) = 0.10 \qquad (36)$$
$$P(40\ \text{MeV}/c^2,\ 9,3) = 0.42$$

There are two comments to be made on the probabilities given in Eqs. 35 and 36. First, 8 of the 9 mass pairs come from events with $3.85 < E_{c.m.} < 4.45$ GeV. As shown in Table II, this energy range constitutes about one quarter of the data. If we use this energy range there is less background and the probabilities are smaller. Specifically for $3.85 < E_{c.m.} < 4.45$ GeV

$$P(16\ \text{MeV}/c^2,\ 8,3) = 0.00047$$
$$P(30\ \text{MeV}/c^2,\ 8,3) = 0.011 \qquad (37)$$
$$P(40\ \text{MeV}/c^2,\ 8,3) = 0.040$$

However, since this $E_{c.m.}$ criteria was set <u>after</u> looking at the data, this is a dangerous way to reduce these probabilities.

The second comment is that our method of calculating the probabilities underestimates them. The method assumes that the positions of the bins on the mass scale are fixed, and then the probability of obtaining the desired peaks in any of these fixed bins is calculated. The method

does not allow for sliding the bins along the mass scale to enhance the peaks in a particular pair of bins. But that is what the eye does in picking out the coincidence of peaks in Fig. 10. We have not corrected the probabilities upward for this effect because the unevenness of the background makes such a correction unreliable.

The probabilities in Eqs. 35-37 are not small enough to demand a non-random explanation of the coincidence of peaks in Fig. 10. An example of a non-random explanation would be a mass 1730 MeV/c^2 particle with $e\gamma$ and $\mu\gamma$ decay modes. And even this explanation does not explain the abnormally narrow width of the peaks. Therefore we conclude that this is a random effect in our data.

7. SUMMARY

Table IV summarizes the 90% confidence upper limits on the branching fractions. We have also given the detection efficiency for each decay mode and the number of events found at the τ mass.

We have not found any decay modes of the τ which violate the concept that the τ and its associated neutrino have a unique, conserved lepton number. This agrees, as do all other published results, with the τ being a sequential lepton.

The upper limits in Table IV are factors of 10 or more smaller than previously measured upper limits[12]. This improvement comes chiefly from the large data sample. Since it is difficult to increase the detector acceptances by more than a factor of 2 or 3, any substantial reduction in these upper limits will require the acquisition of a yet larger data sample.

We have not found any evidence for the existence of leptons which decay via $e^* \to e + \gamma$ or $\mu^* \to \mu + \gamma$ up to a mass of 3.3 GeV/c^2.

This work was supported by the U. S. Department of Energy under Contract Nos. DE-AC03-76SF00515 and W-7405-ENG-48.

TABLE I. The probability of a $\pi^{\pm}$ being called an $e^{\pm}$, P ($\pi \to e$): and the probability of an $e^{\pm}$ being correctly identified, P($e \to e$); using the liquid argon electromagnetic shower detector and the time-of-flight counters.

Momentum (GeV/c)	P($\pi \to e$)	P($e \to e$)
.3- .4	$.098 \pm .007$	$.730 \pm .007$
.4- .5	$.111 \pm .007$	$.760 \pm .009$
.5- .6	$.069 \pm .006$	$.833 \pm .011$
.6- .7	$.056 \pm .006$	$.866 \pm .012$
.7- .8	$.032 \pm .006$	$.823 \pm .017$
.8- .9	$.052 \pm .009$	$.857 \pm .018$
.9-1.1	$.031 \pm .002$	$.848 \pm .015$
1.1-1.3	$.036 \pm .004$	$.918 \pm .015$
1.3-1.5	$.056 \pm .010$	$.968 \pm .008$

TABLE II. Tau pair production vs. center of mass energy.

Interval (GeV)	Integrated Luminosity (nb^{-1})	Number of Produced $\tau^+\tau^-$ Pairs
3.85-4.25	2129	7348
4.25-4.65	1788	6248
4.65-5.05	1866	6006
5.05-5.45	6176	18136
5.45-6.35	1221	2922
6.35-6.85	3783	7448
Total:	16963	48108

TABLE III. 90% confidence level upper limit on tau → 3 charged lepton decays.

Decay	Type	Average Acceptance(%)	Number Detected Events	Branching Ratio Upper Limit(%)
μμμ	μxx	15.7	8	.086
	μμx	4.6	0	.052
	μμμ	.28	0	.86
eμμ	μxx	5.4	9	.28
	exx	7.1	13	.28
	μμx	.87	0	.28
	eμx	5.8	0	.042
	eμμ	.68	0	.35
μee	μxx	1.5	4	.56
	exx	7.1	13	.38
	μex	3.4	0	.070
	eex	4.2	1	.10
	μee	1.7	0	.14
eee	exx	5.8	24	.57
	eex	7.3	1	.056
	eee	2.8	0	.086

TABLE IV: 90% confidence level upper limits on τ decay modes. The detector acceptance for each mode is given in column 3; and the number of events found within the τ mass resolution is given in column 4. The limits include the charge conjugate decay modes.

Decay Mode $\tau^- \rightarrow$	Upper Limit on Branching Fraction	Acceptance (%)	Number Events Found at τ Mass
$\mu^-+\gamma$	5.5×10^{-4}	7.3	1
$e^-+\gamma$	6.4×10^{-4}	6.3	1
$\mu^-+\mu^+\mu^-$	4.9×10^{-4}	4.9	0
$e^-+\mu^+\mu^-$	3.3×10^{-4}	7.3	0
$\mu^-+e^+e^-$	4.4×10^{-4}	9.3	1
$e^-+e^+e^-$	4.0×10^{-4}	10.1	1
$\mu^-+\pi^o$	8.2×10^{-4}	2.9	0
$e^-+\pi^o$	$21. \times 10^{-4}$	3.5	3
μ^-+K^o	$10. \times 10^{-4}$	2.4	0
e^-+K^o	$13. \times 10^{-4}$	3.1	1
$\mu^-+\rho^o$	4.4×10^{-4}	5.5	0
$e^-+\rho^o$	3.7×10^{-4}	6.5	0

TABLE V. 90% confidence level upper limit on R_{μ^*}.

Mass Interval (GeV/c^2)	Maximum Bin Sum	90% Confidence Level Upper Limit on R_{μ^*}
.6-1.6	3	.0010
1.6-2.1	5	.0014
2.1-2.5	6	.0025
2.5-2.9	3	.0043
2.9-3.2	3	.0090
3.2-3.3	1	.0193

TABLE VI. 90% confidence level upper limit on R_{e^*}.

Mass Interval (GeV/c^2)	Maximum Bin Sum	90% Confidence Level Upper Limit on R_{e^*}
.5- .6	0	.0014
.6- .8	3	.0027
.8-1.0	5	.0023
1.0-1.3	8	.0025
1.3-2.0	22	.0041
2.0-2.3	15	.0030
2.3-2.5	16	.0051
2.5-3.0	10	.0096
3.0-3.2	1	.0039
3.2-3.3	0	.0110

FOOTNOTES AND REFERENCES

1. M. L. Perl, Ann. Rev. Nucl. Part. Sci. 30, 299 (1980).

2. G. Flugge, Z. Phys. C1, 121 (1979).

3. Y. S. Tsai, Phys. Rev. D4, 2821 (1971).

4. H. B. Thacker and J. J. Sakurai, Phys. Lett. B36, 103 (1971).

5. K. G. Hayes, Ph.D. Thesis, Stanford University (1981); SLAC Report 237 (1981).

6. R. H. Schindler, Ph.D. Thesis, SLAC Report No. 219 (1979).

7. G. S. Abrams et al., IEEE Trans. Nucl. Sci. NS-27,59 (1980).

8. T. M. Himel, Ph.D. Thesis, SLAC Report No. 223 (1979).

9. The acoplanarity angle is defined by
arccos $[(\underset{\sim}{u}_1 \times \underset{\sim}{u}_b) \cdot (\underset{\sim}{u}_2 \times \underset{\sim}{u}_b)] / |\underset{\sim}{u}_1 \times \underset{\sim}{u}_b| |\underset{\sim}{u}_2 \times \underset{\sim}{u}_b|$
where u_1, u_2, u_b, are unit vectors in the direction of each of the final particles and of the beam respectively.

10. For a recent reference see M. L. Perl, New Phenomena in Lepton-Hadron Physics (Plenum Press, New York, 1979), ed. by D.E.C.Fries and J. Wess, page 115.

11. C. Bacci et al, Phys. Lett. 71B, 227 (1977); 44B, 530 (1973).

12. M. L. Perl, Proc. of 1977 Int. Symp. on Lepton and Photon Interactions at High Energies (DESY, Hamburg, 1977) p. 145.

FIGURE CAPTIONS

1. Cross sectional view of the Mark II detector. A) vacuum chamber, B) pipe counter, C) 16 layer drift chamber, D) time of flight counters, E) solenoid coil, f) lead-liquid argon shower detectors, G) iron flux return and hadron absorber , H) muon proportional tubes.

2. Isometric projection view of the Mark II detector.

3. Measured efficiency for photon detection of the liquid argon shower detector. The curve is a Monte Carlo calculation of that efficiency.

4. Cross sectional view of a muon system proportional tube module containing eight tubes.

5. Probability in percent of a pion being misidentified as a muon.

6. The μ-γ mass resolution as a function of E_μ/E_{beam}.

7. The ℓ-γ invariant mass distributions before the application of background removing constraints.

8. The acceptance for detecting a) $\tau \to e+\gamma$ and b) $\tau \to \mu+\gamma$. The solid and dash-dot curves are before and after the application of background removing constraints.

9. The ℓ-γ invariant mass distributions after the application of background removing constraints. The arrow indicates the position of the τ mass 1.782 GeV/c^2.

10. The ℓ-γ invariant mass distributions in the neighborhood of the tau mass after the application of background removing constraints. The mass resolution function curve is centered on the τ mass of 1.782 GeV/c^2.

11. Acceptance for $\tau \to \mu ee$ for various observed particle combinations.

12. The $e^{\pm}e^{+}e^{-}$ invariant mass distributions. The arrow indicates the position of the τ mass 1.782 GeV/c^2.

13. The $\mu^{\pm}e^{+}e^{-}$ invariant mass distributions. The arrow indicates the position of the τ mass 1.782 GeV/c^2.

14. The $e^{\pm}\mu^{+}\mu^{-}$ invariant mass distributions. The arrow indicates the position of the τ mass 1.782 GeV/c^2.

15. The $\mu^{\pm}\mu^{+}\mu^{-}$ invariant mass distributions. The arrow indicates the position of the τ mass 1.782 GeV/c^2.

16. The $\pi^{+}\pi^{-}$ invariant mass for $\mu^{-}(\pi^{+}\pi^{-})$ candidates. The curve is a Breit-Wigner distribution for the ρ^{o}.

17. The $\ell+\rho^o$ invariant mass distributions. The arrow indicates the position of the τ mass 1.782 GeV/c^2.

18. The $\ell+\rho^o$ invariant mass distributions in the neighborhood of the τ mass. The mass resolution function curve is centered on the τ mass 1.782 GeV/c^2.

19. The $\pi^+\pi^-$ invariant mass distribution for $\ell+K^o$ candidate events.

20. The $\ell+K^o$ invariant mass distributions. The arrow indicates the position of the τ mass 1.782 GeV/c^2.

21. The calculated π^o mass resolution, σ, for various values of the assymetry parameter a, defined in Eq. 28.

22. The $Y = (E_\ell + E_{\pi o} - E_{beam})/\sigma(E_\ell + E_{\pi o})$ distribution for $\ell+\pi^o$ candidates. The curve is the calculated distribution for the $\tau \to \ell+\pi^o$.

23. The $\ell+\pi^o$ invariant mass distributions before the application of background reducing constraints.

24. The $\ell+\pi^o$ invariant mass distributions after the application of background reducing constraints. The arrow indicates the position of the τ mass 1.782 GeV/c^2.

25. The width of the mass resolution function containing 80% of the detected events for $\mu^* \to \mu + \gamma$ as a function of $\text{mass}_{\mu^*}/E_{beam}$.

26. The acceptance for $\mu^* \to \mu+\gamma$ as a function of $\text{mass}_{\mu^*}/E_{beam}$.

27. Number of $\mu^* \to \mu+\gamma$ events which would have been detected if $R(e^+e^- \to \mu^*+\mu^{*-}) = 1$ versus the μ^* mass.

28. The $e-\gamma$ invariant mass distribution for $e^+ + e^- \to e^{*+} + e^{*-}$ candidates.

29. Number of $e^* \to e+\gamma$ events which would have been detected if $R(e^+e^- \to e^*+e^{*-}) = 1$ versus the e^* mass.

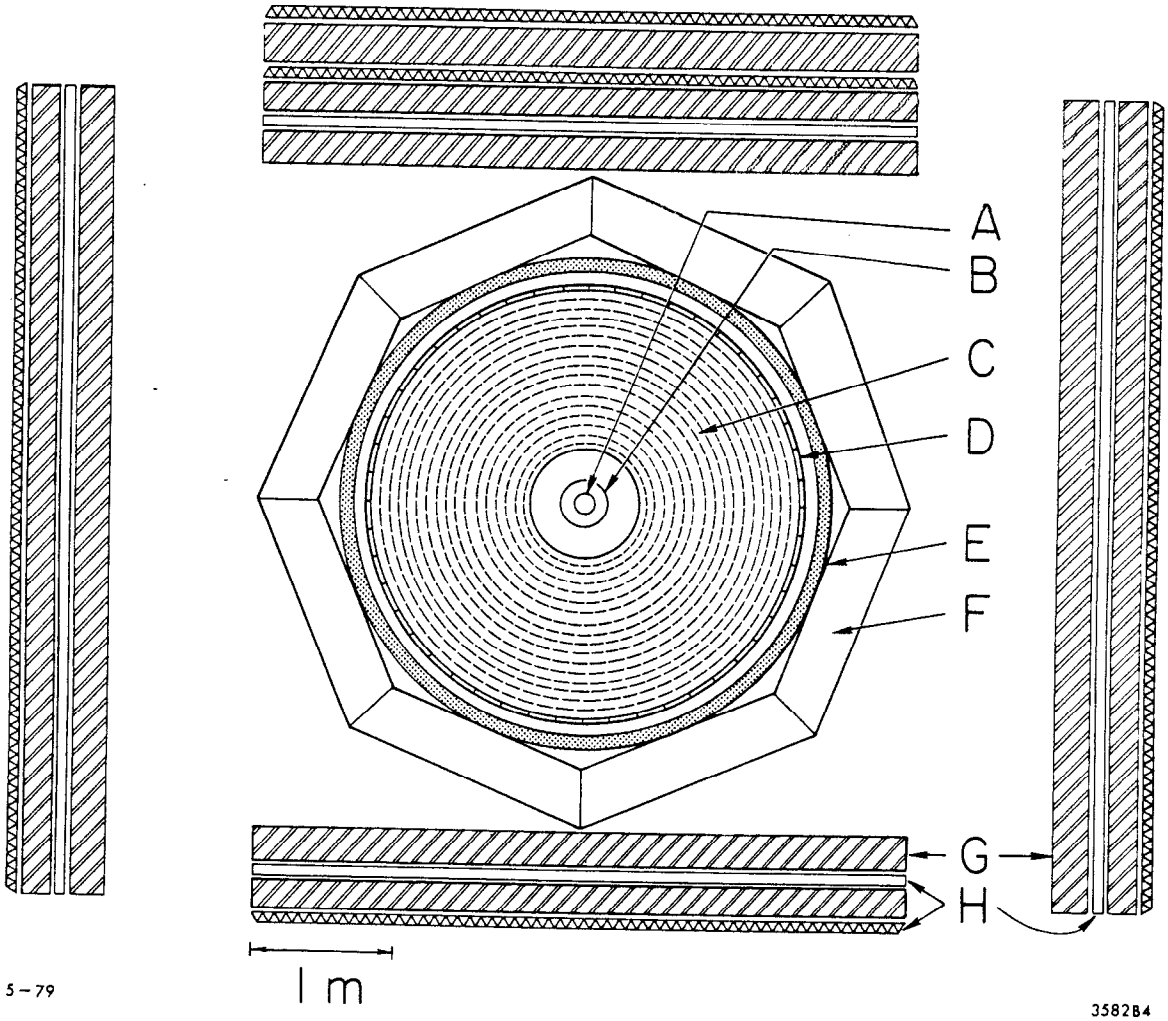

Fig. 1

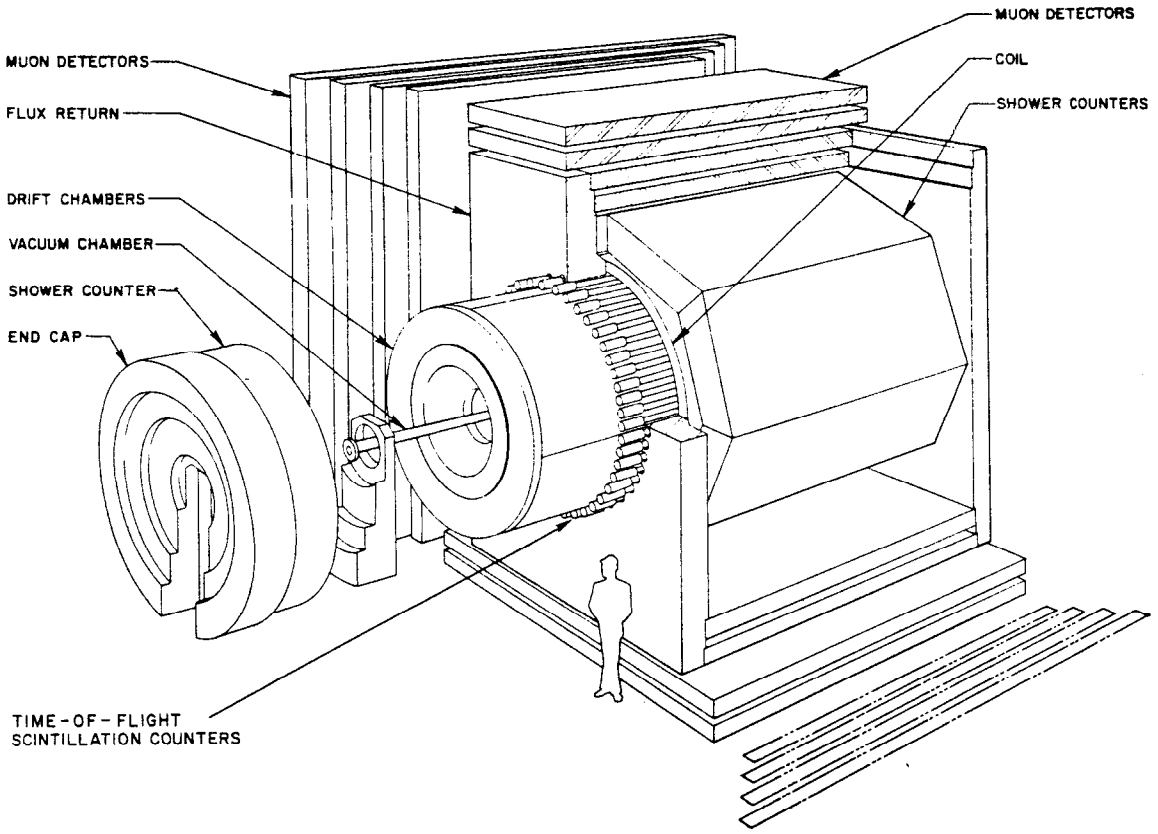

7-78

3418A22

Fig. 2

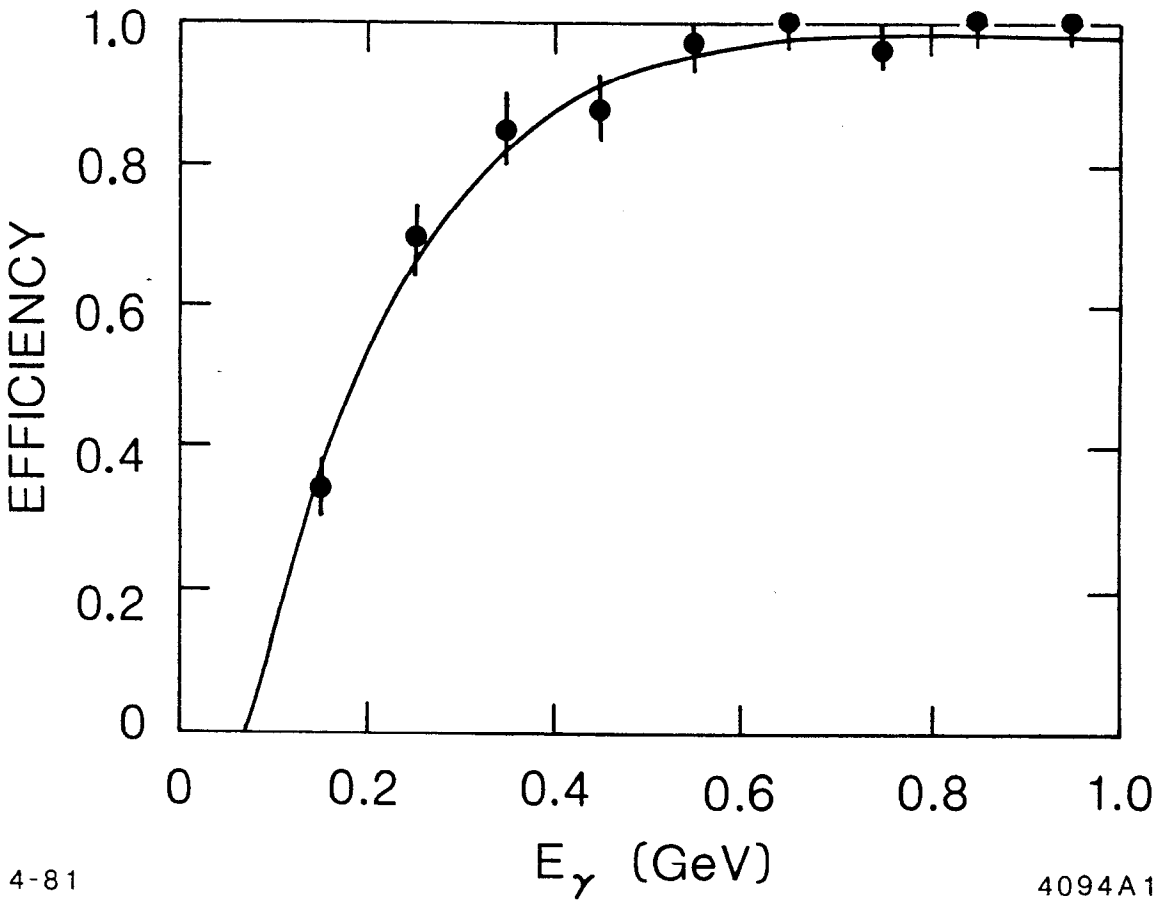
1.0
0.8
0.6
0.4
0.2
0
EFFICIENCY
0
0.2
0.4
0.6
0.8
1.0
E_γ (GeV)
4-81
4094A1

Fig. 3

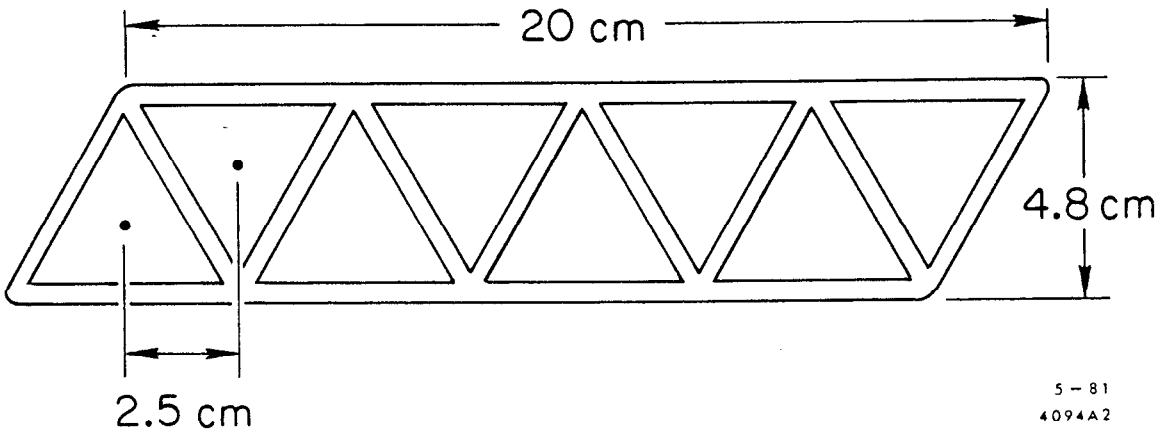

Fig. 4

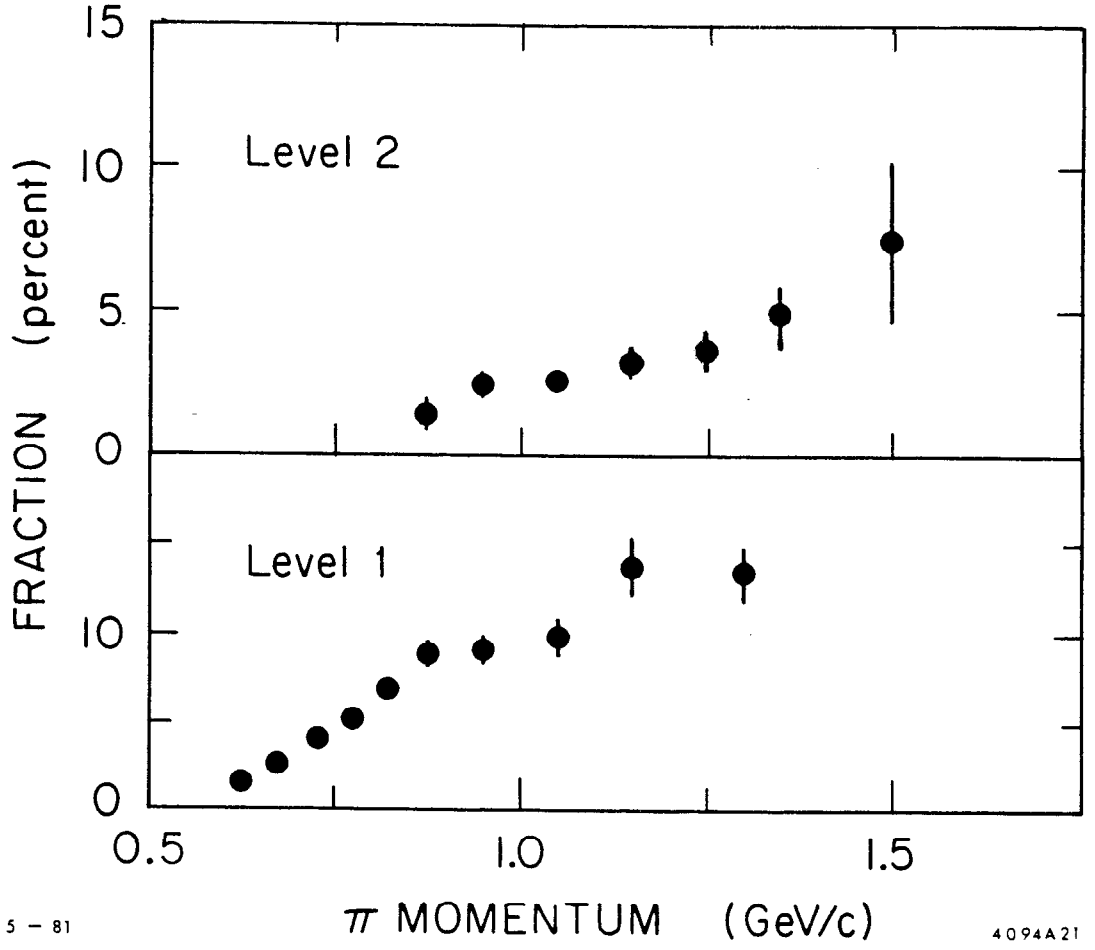
15
10
5
0
Level 2
Level 1
10
0
FRACTION (percent)
0.5
1.0
1.5
π MOMENTUM (GeV/c)
5 – 81
4094A21

Fig. 5

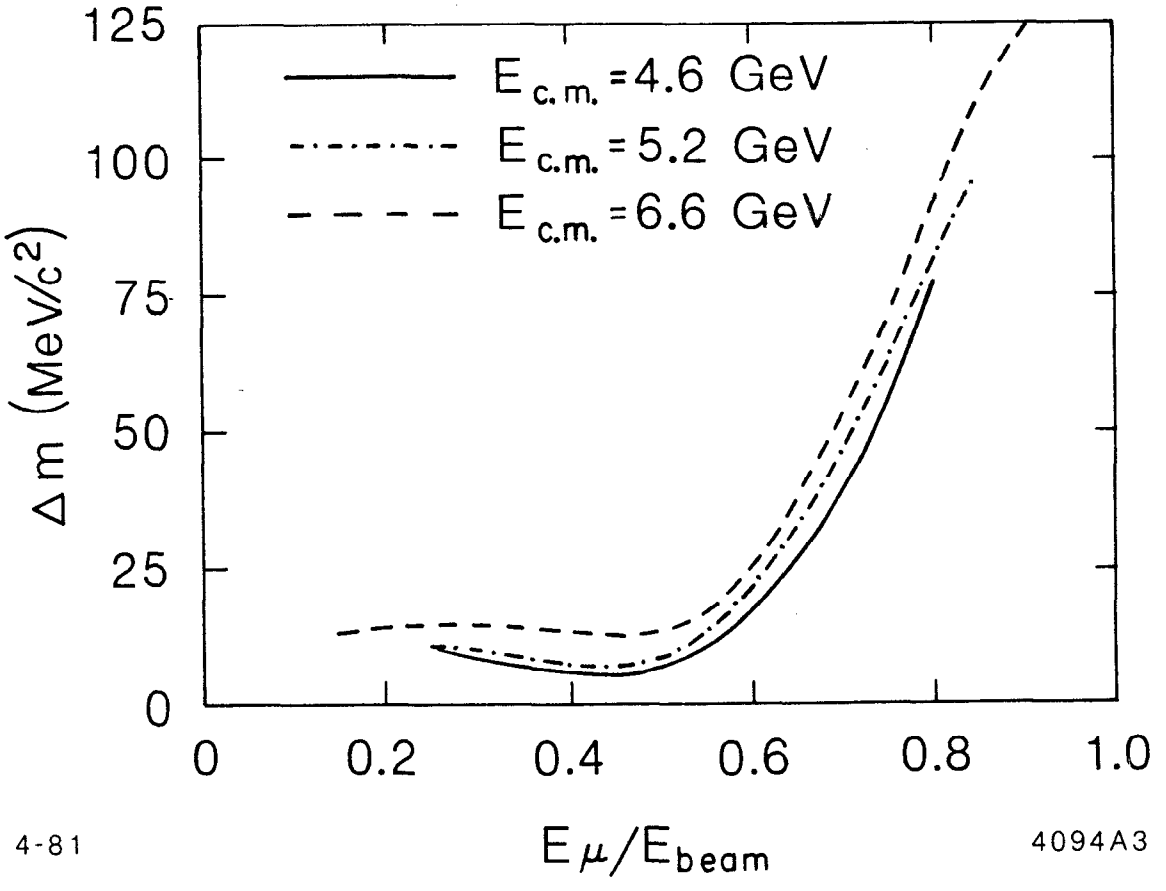
125
100
75
50
25
0
Δ m (MeV/c²)
E c.m. = 4.6 GeV
E c.m. = 5.2 GeV
E c.m. = 6.6 GeV
0
0.2
0.4
0.6
0.8
1.0
Eμ/Ebeam
4-81
4094A3

Fig. 6

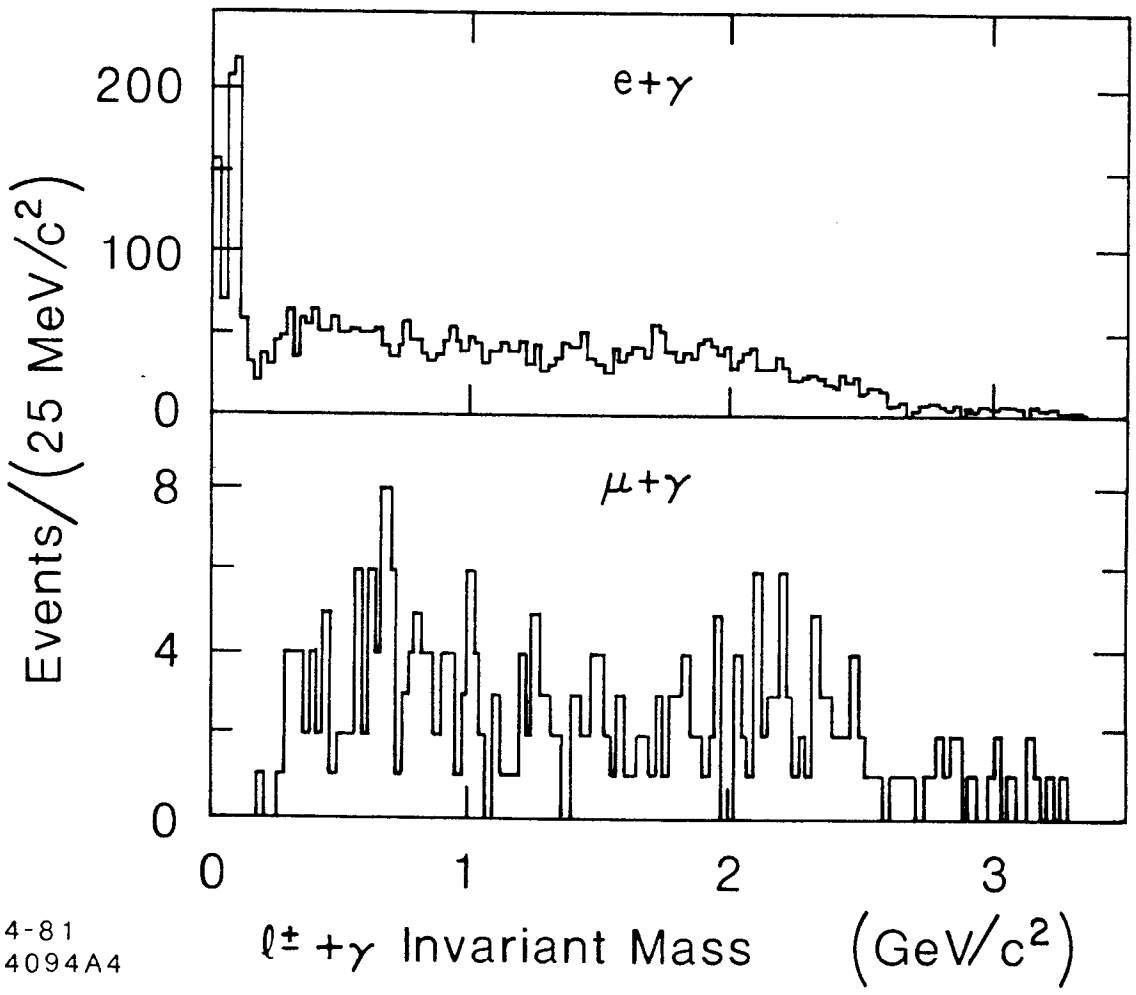
200
100
0
e+γ
Events/(25 MeV/c²)
8
4
0
μ+γ
0
1
2
3
4-81
4094A4
ℓ± +γ Invariant Mass (GeV/c²)

Fig. 7

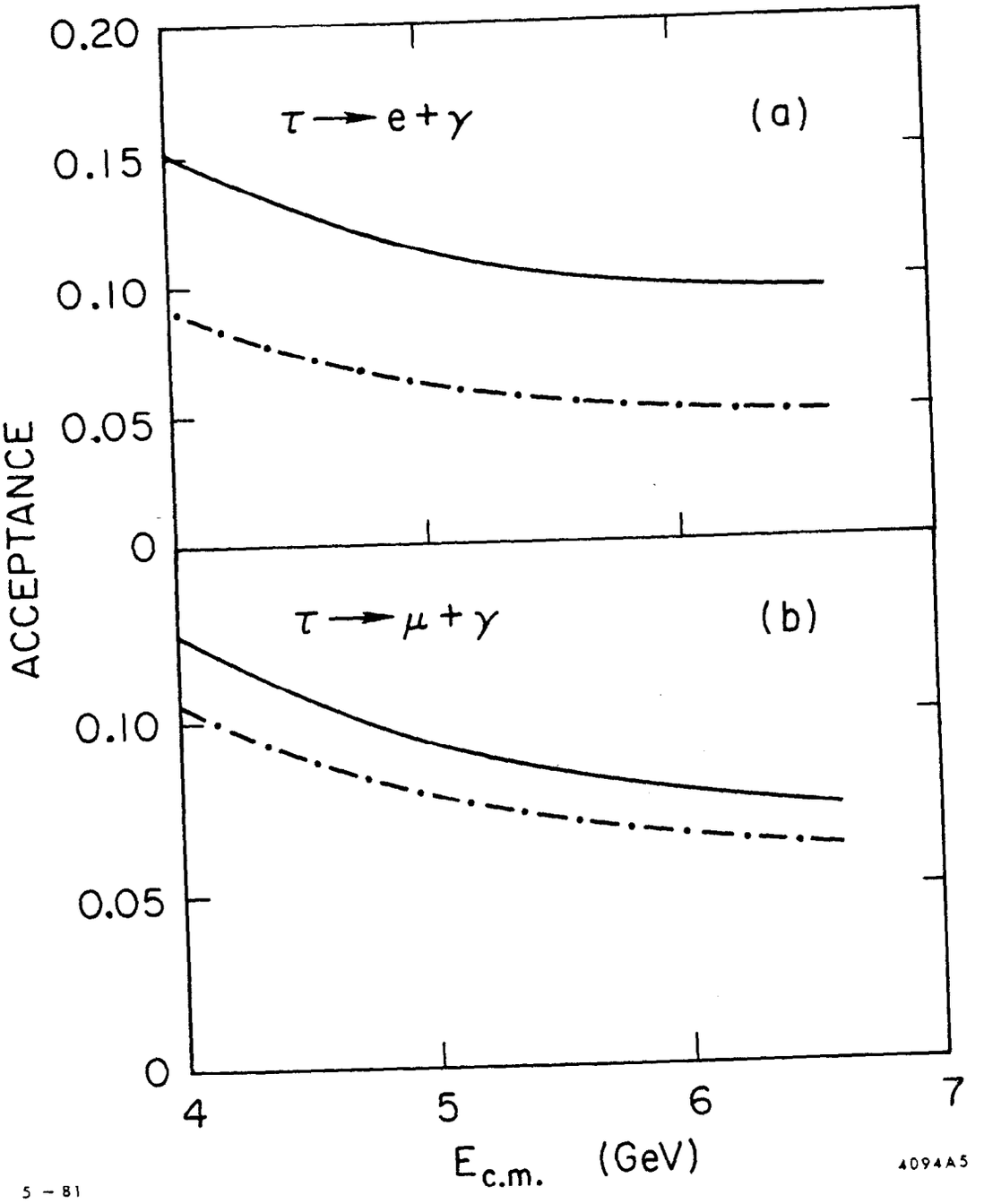
0.20
0.15
0.10
0.05
0
τ → e + γ
(a)
τ → μ + γ
(b)
ACCEPTANCE
0.10
0.05
0
4
5
6
7
E c.m. (GeV)
4094A5

5 – 81

Fig. 8

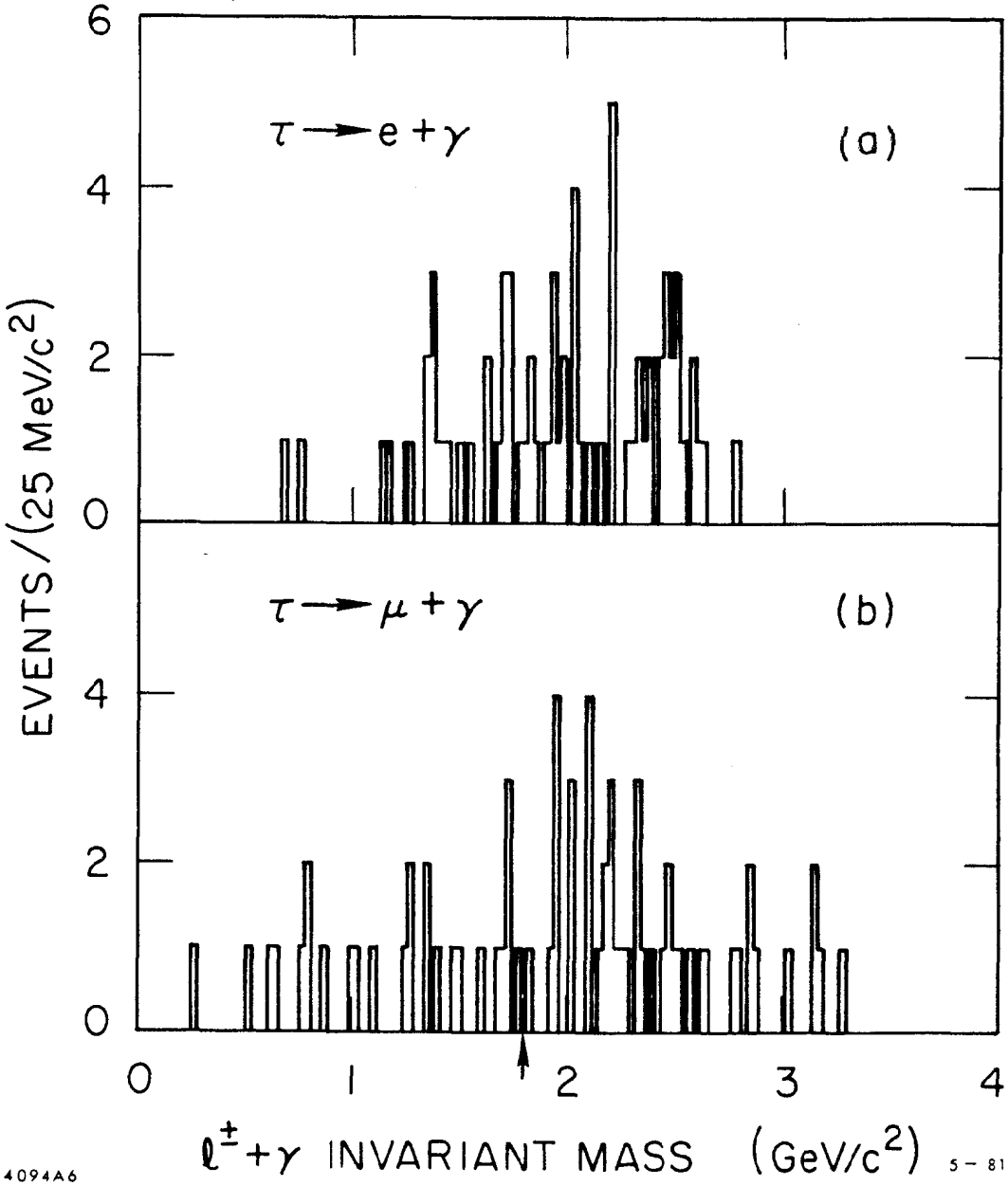
6
4
2
0
$\tau \rightarrow e + \gamma$
(a)
$\tau \rightarrow \mu + \gamma$
(b)
EVENTS/(25 MeV/c^2)
0
1
2
3
4
$\ell^{\pm} + \gamma$ INVARIANT MASS (GeV/c^2)
4094A6
5-81

Fig. 9

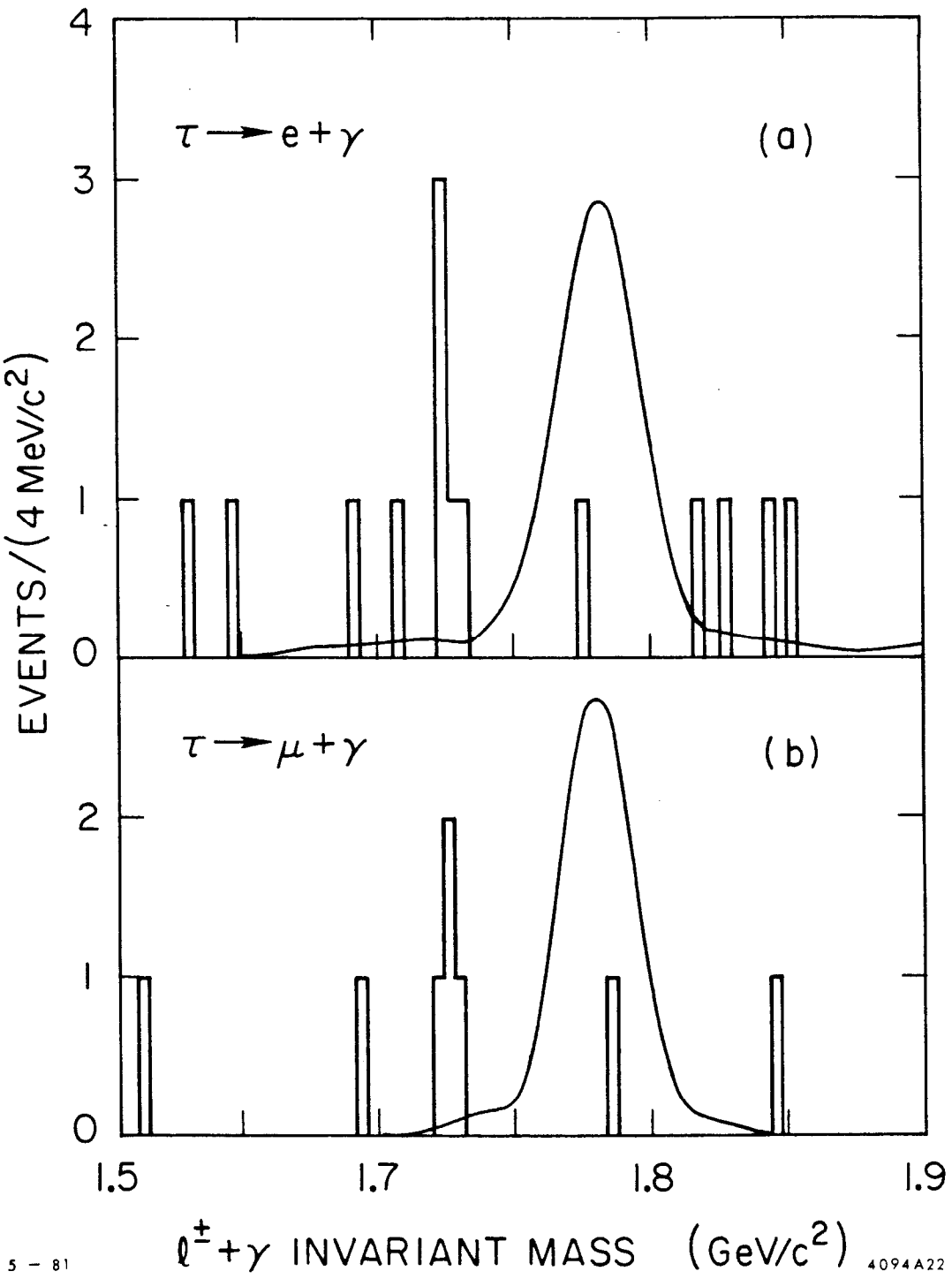
τ → e + γ
(a)
τ → μ + γ
(b)
EVENTS/(4 MeV/c²)
0
1
2
3
4
1.5
1.7
1.8
1.9
ℓ± + γ INVARIANT MASS (GeV/c²)
5 - 81
4094A22

Fig. 10

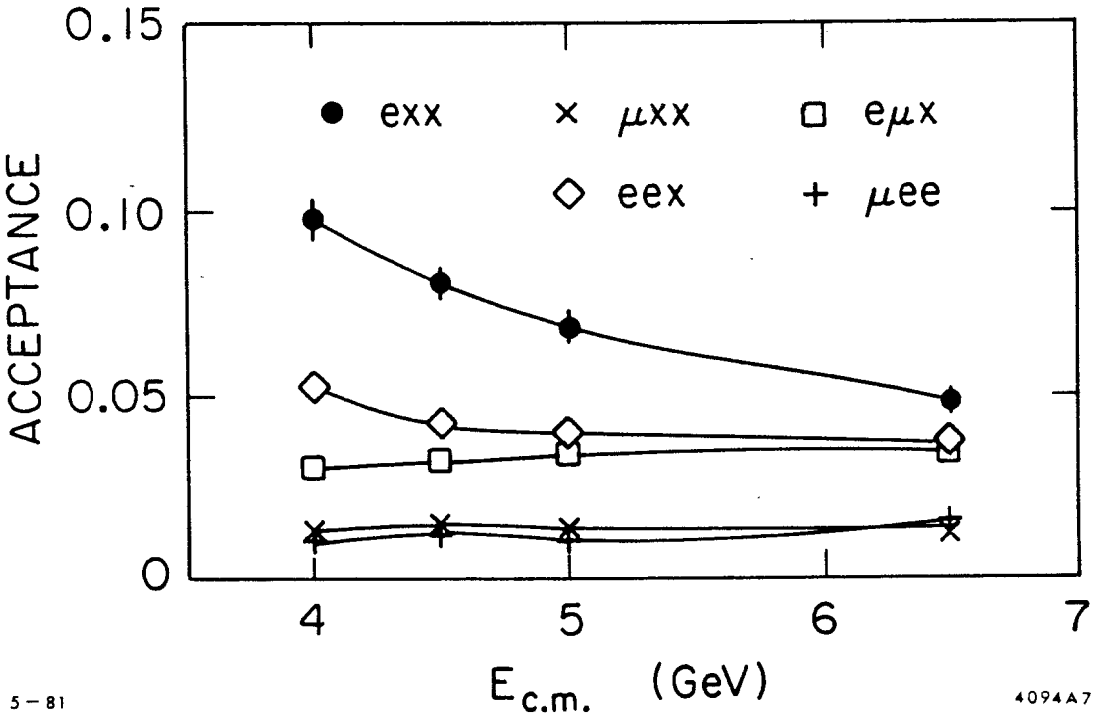
0.15
0.10
0.05
0
ACCEPTANCE
exx
μxx
eμx
eex
μee
4
5
6
7
E c.m. (GeV)
5-81
4094A7

Fig. 11

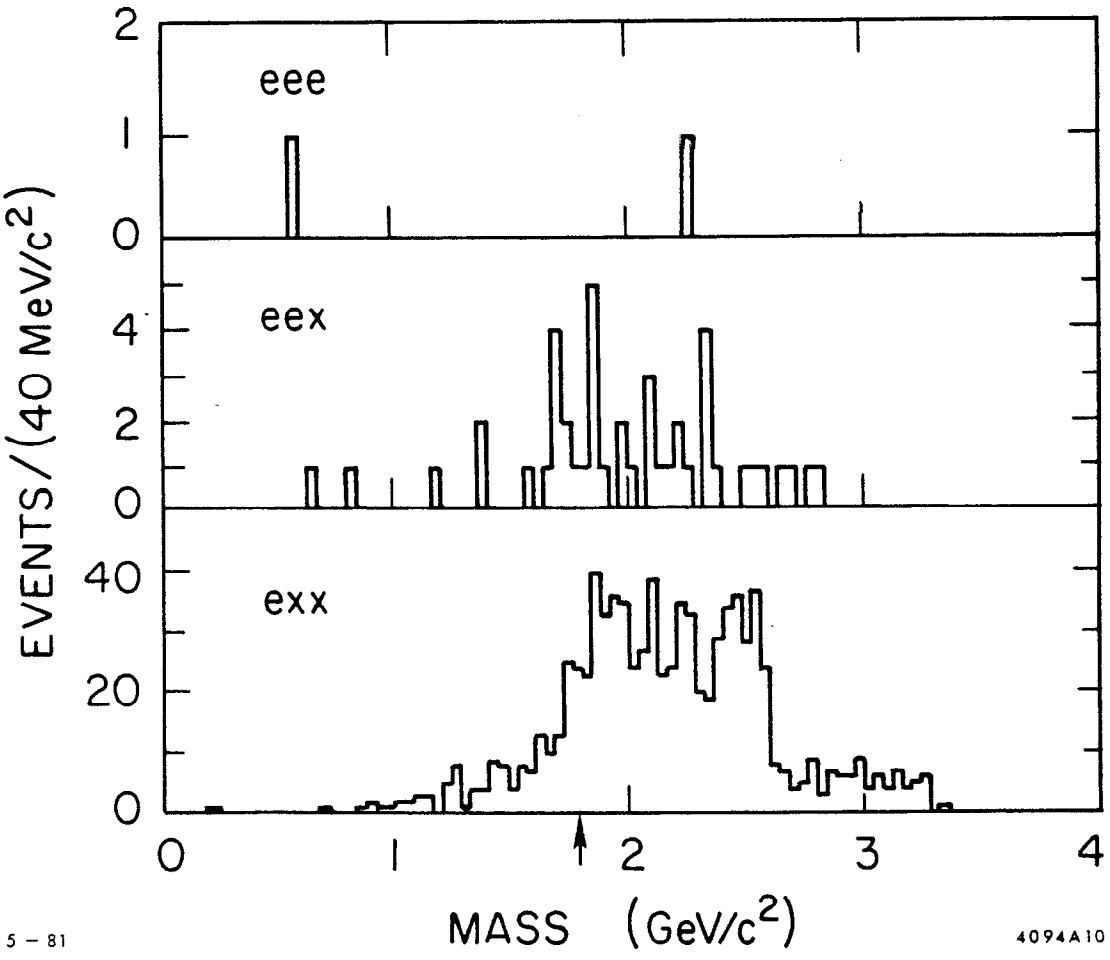

Fig. 12

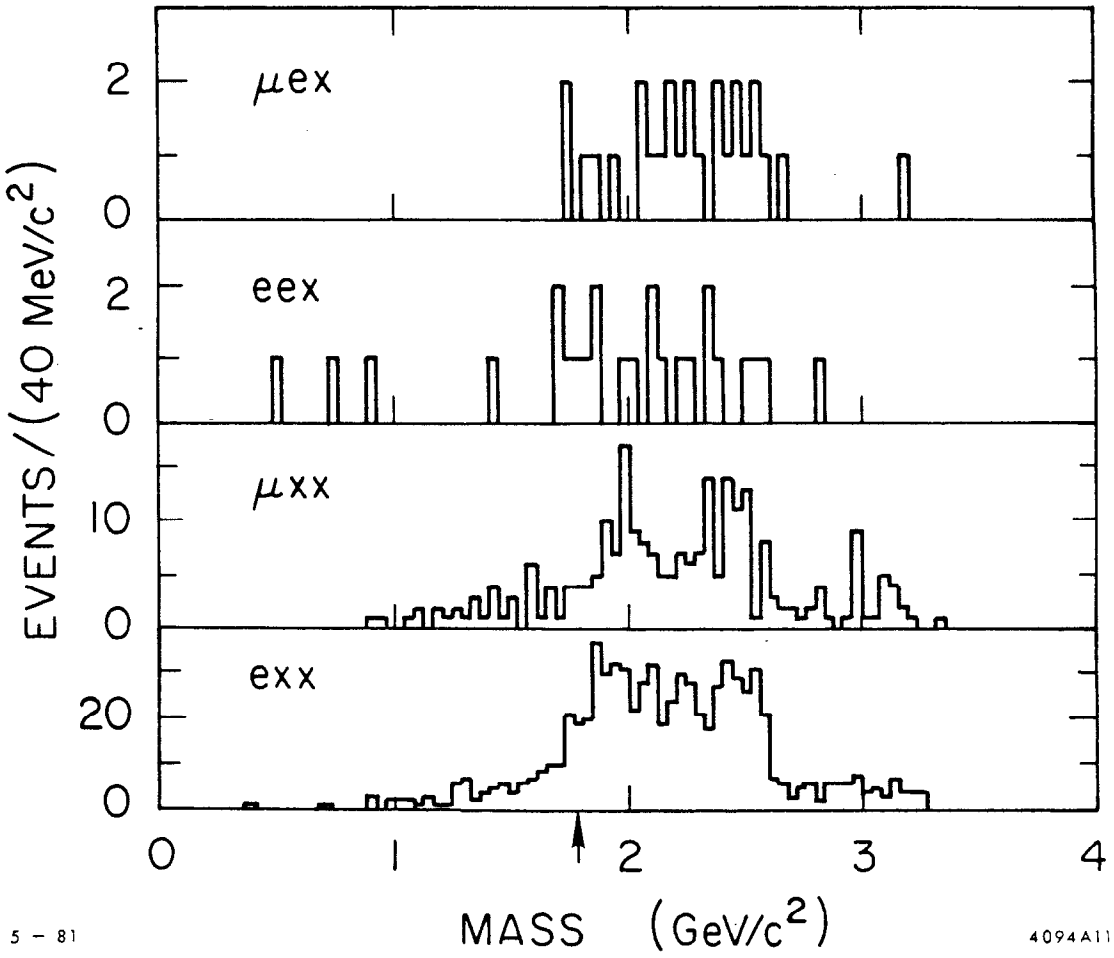

Fig. 13

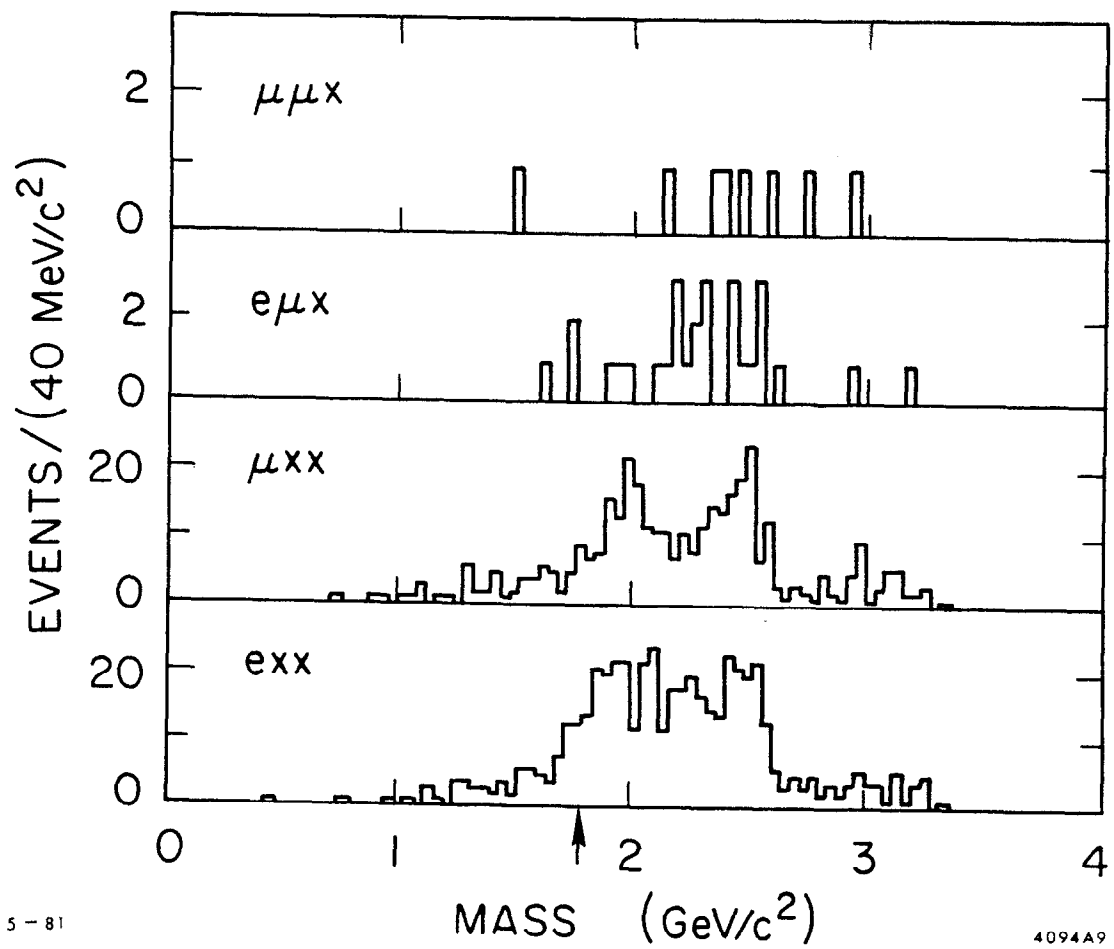
μμx
eμx
μxx
exx
2
0
2
0
20
0
20
0
EVENTS/(40 MeV/c²)
0
1
2
3
4
MASS (GeV/c²)
5 - 81
4094A9

Fig. 14

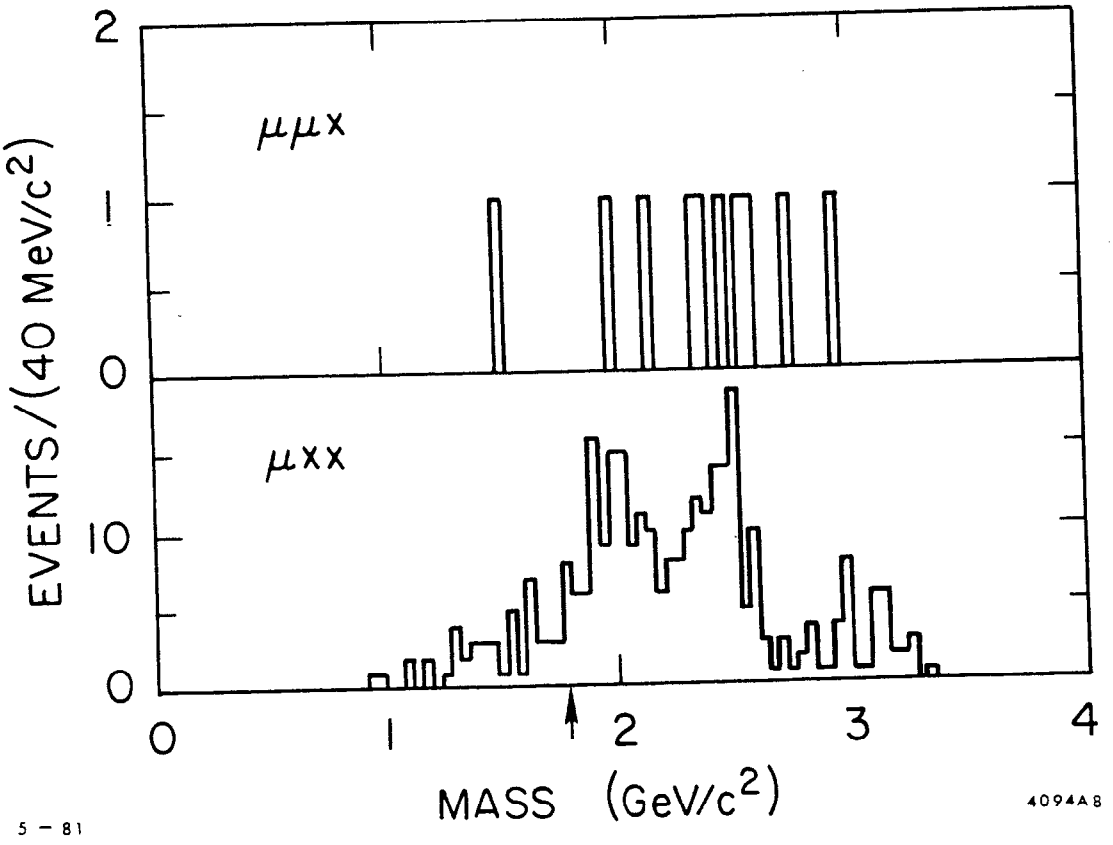

Fig. 15

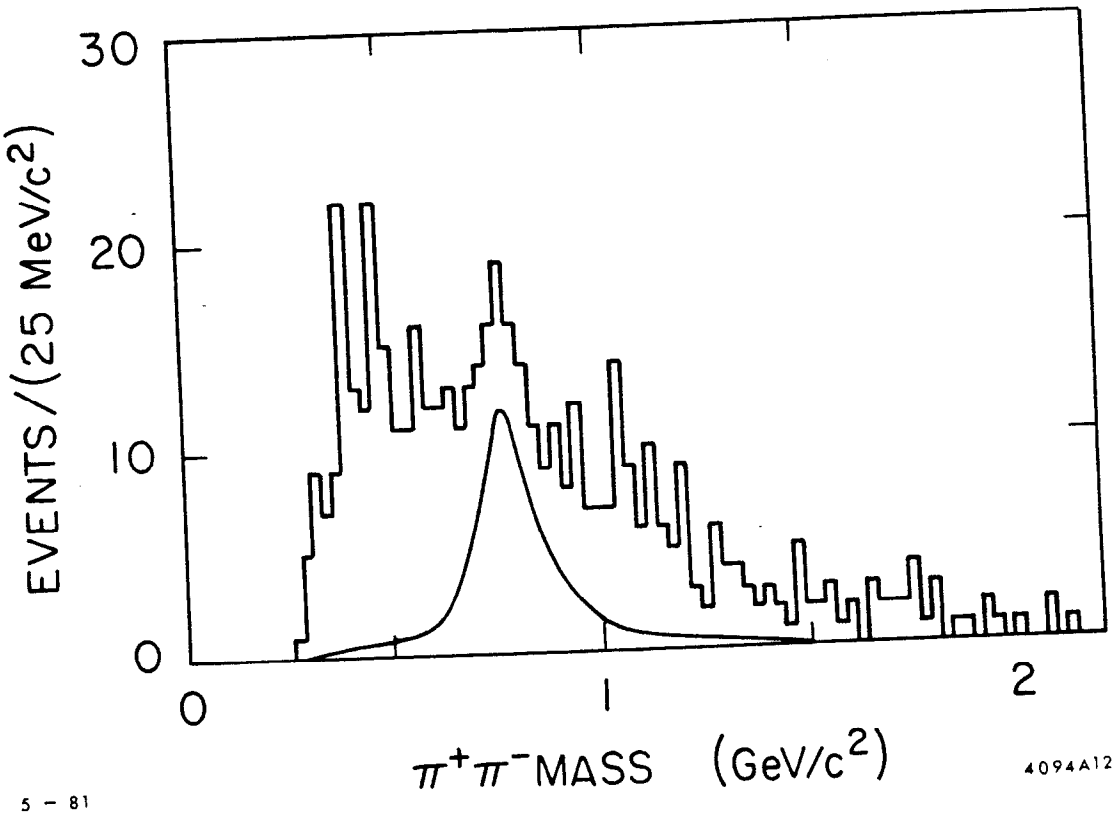

Fig. 16

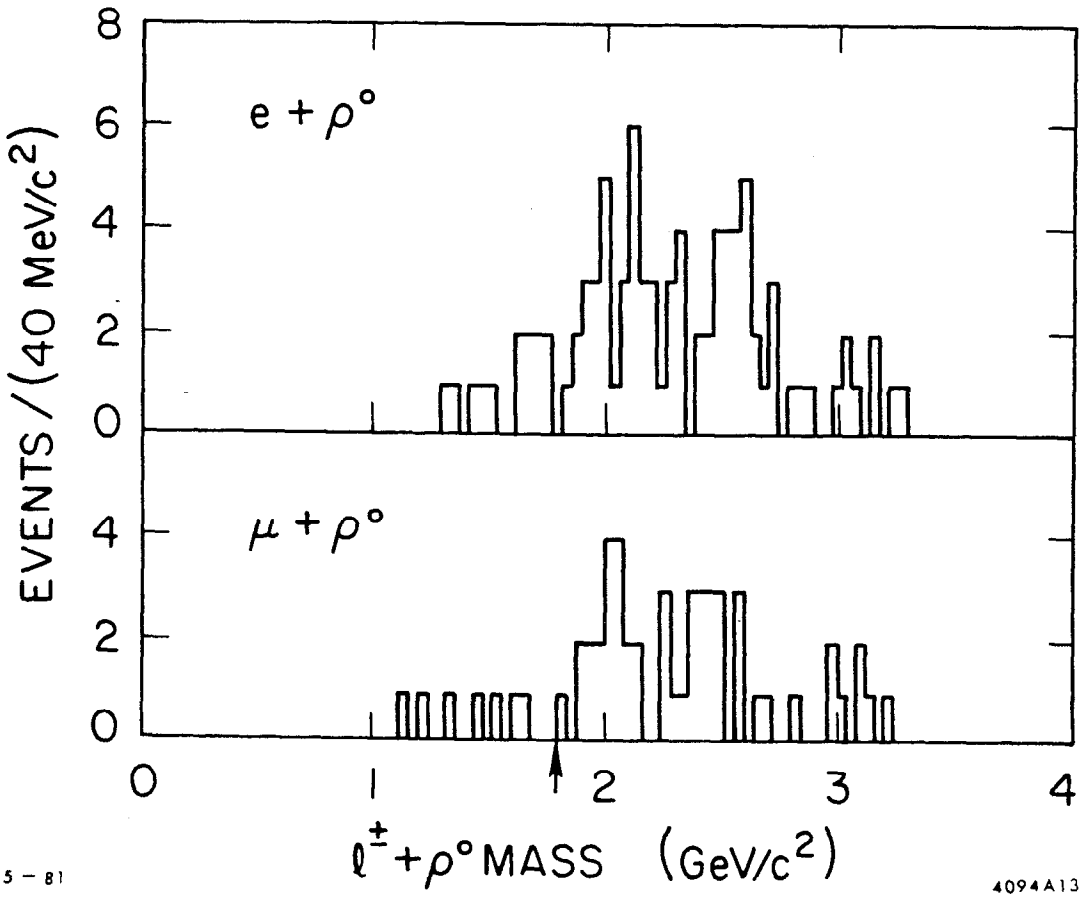

Fig. 17

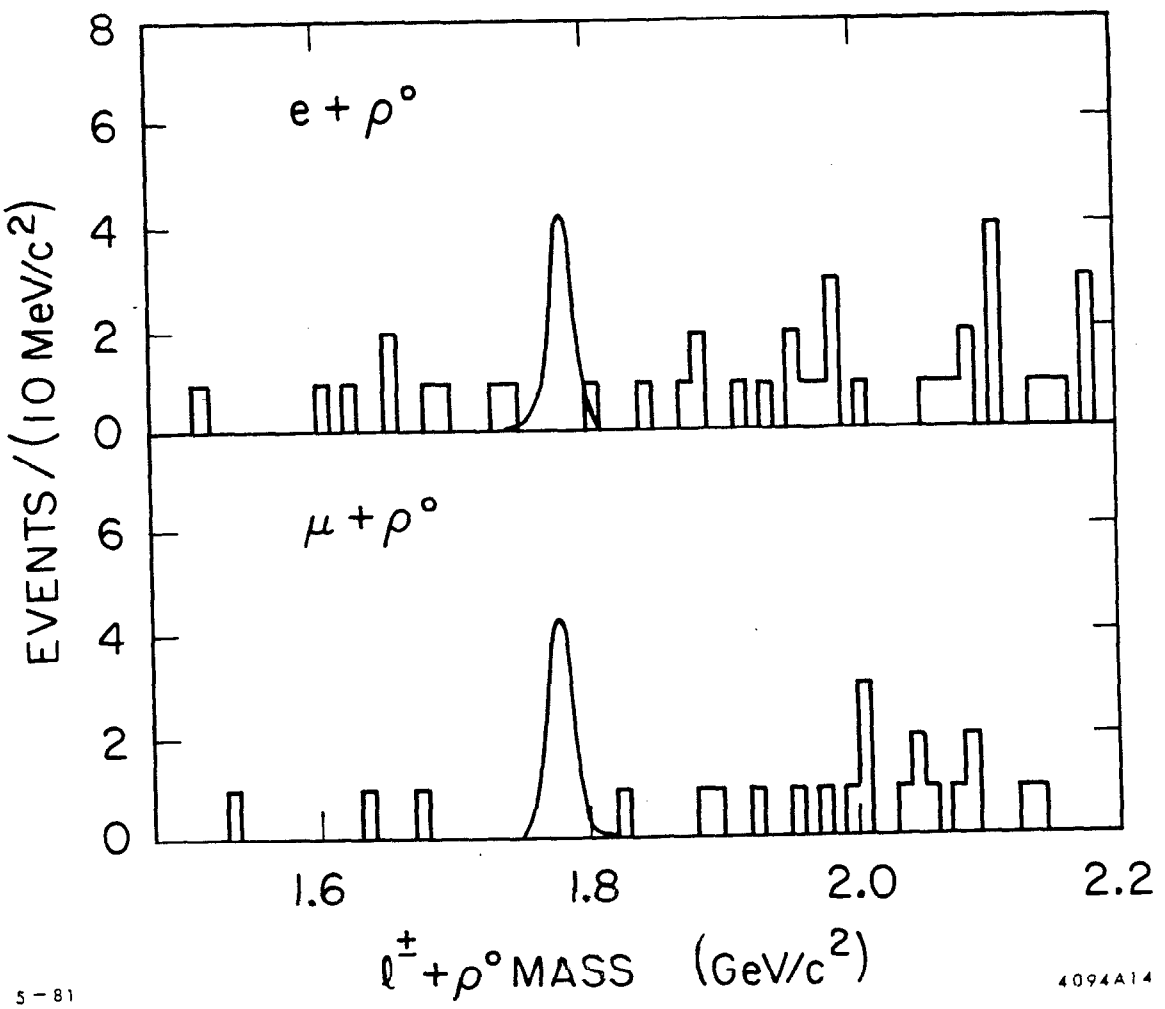
e + ρ°
μ + ρ°
EVENTS / (10 MeV/c²)
8
6
4
2
0
6
4
2
0
1.6
1.8
2.0
2.2
l± + ρ° MASS (GeV/c²)
5 – 81
4094A14

Fig. 18

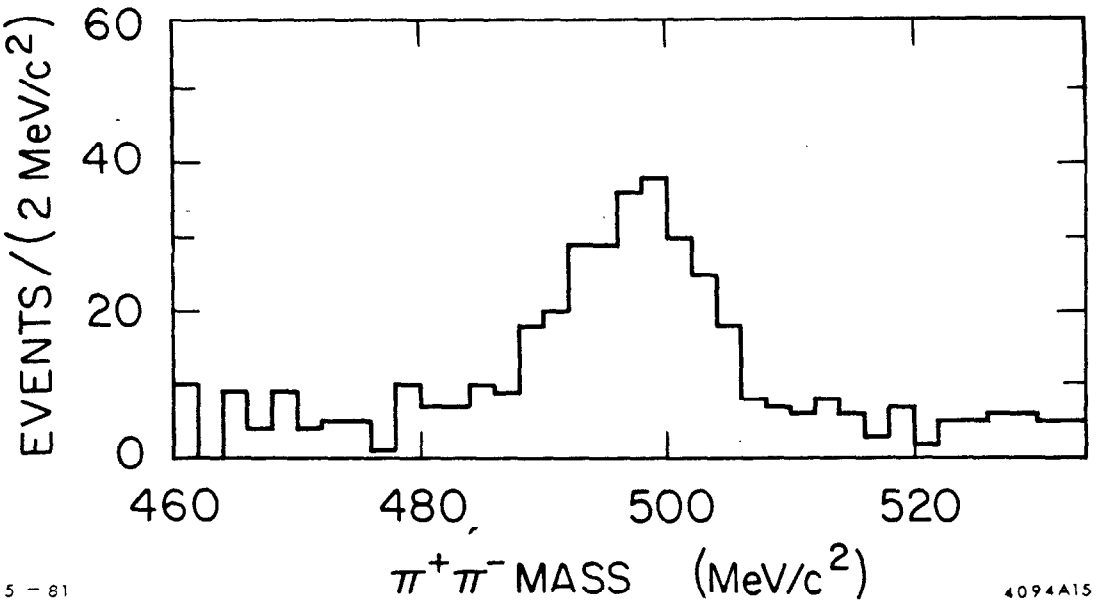
EVENTS/(2 MeV/c²)
60
40
20
0
460
480
500
520
π⁺π⁻ MASS (MeV/c²)
5 – 81
4094A15

Fig. 19

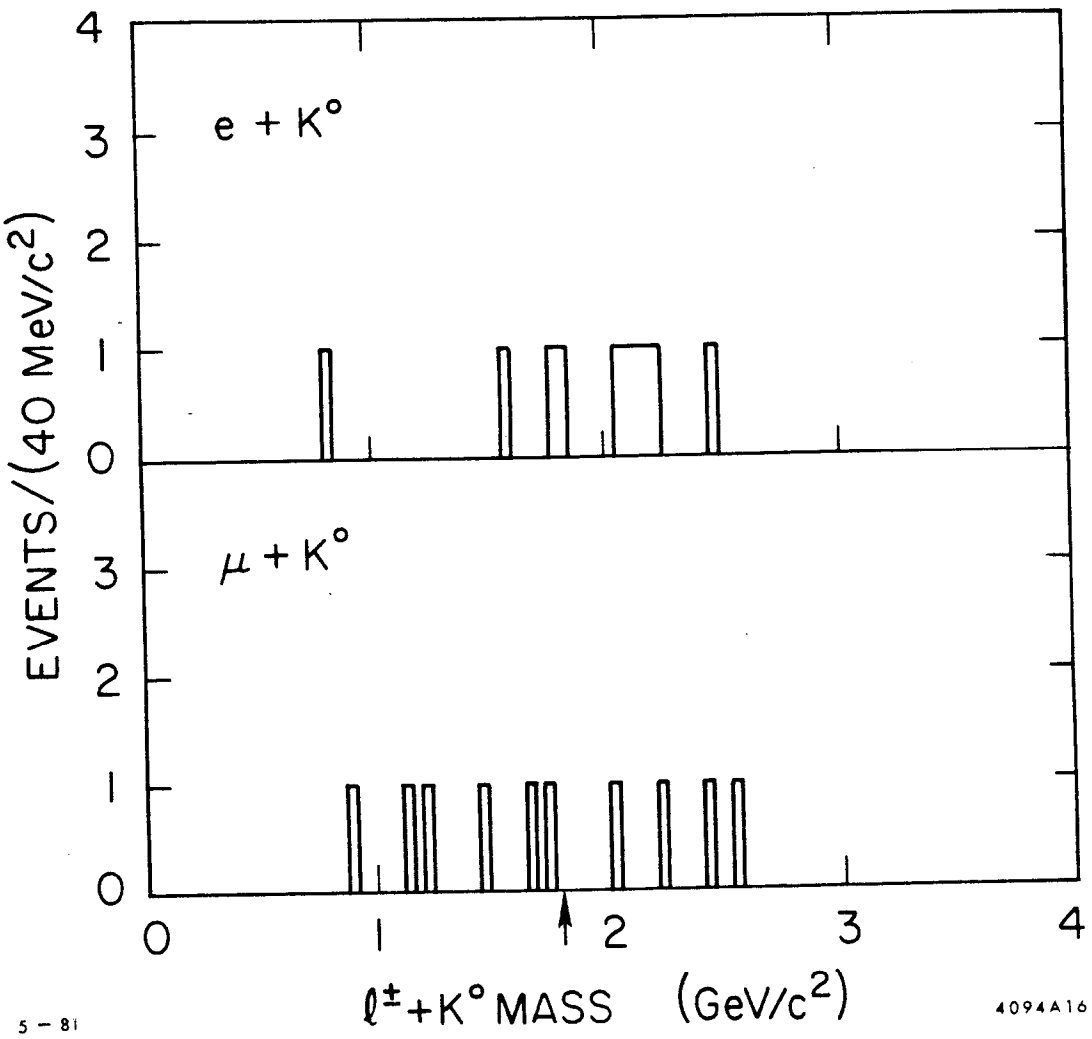

Fig . 20

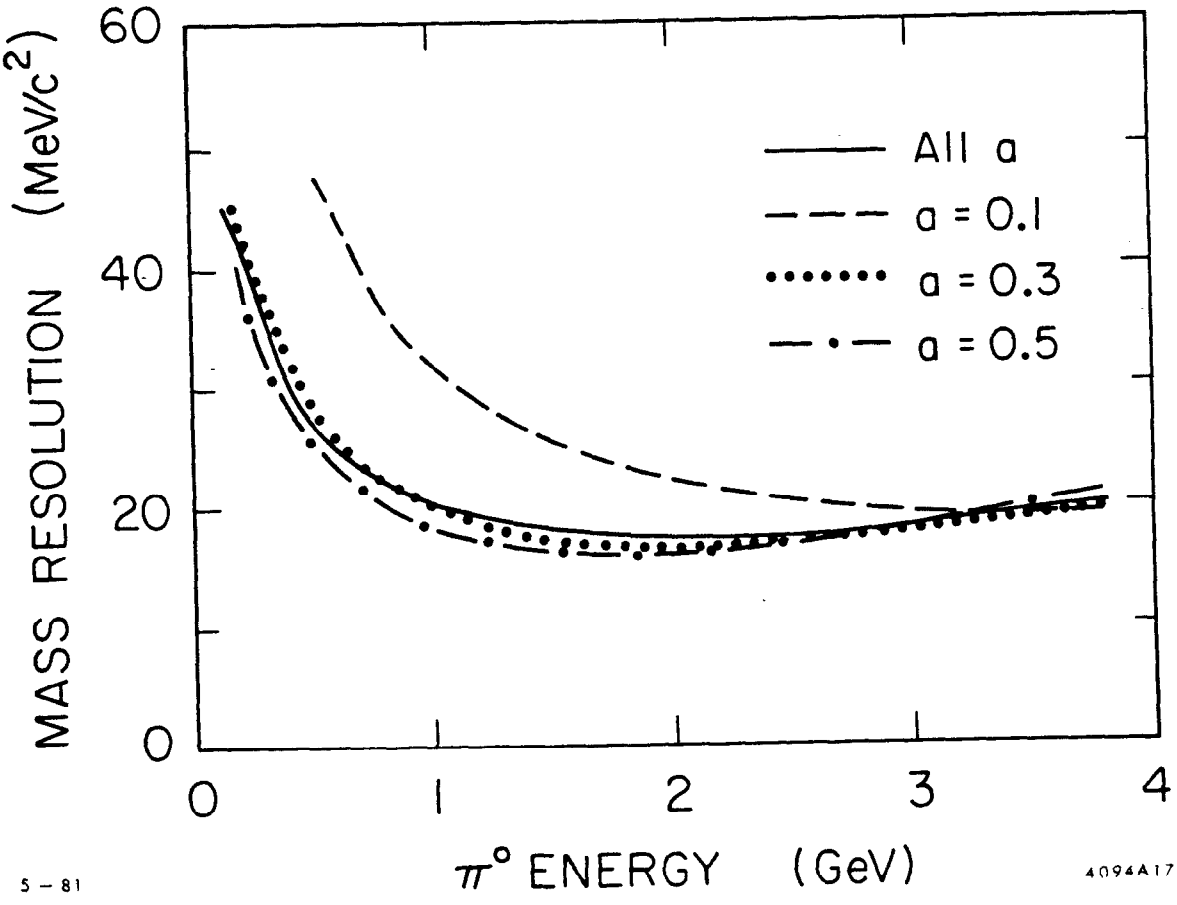
MASS RESOLUTION (MeV/c²)
60
40
20
0
0
1
2
3
4
π° ENERGY (GeV)
All a
a = 0.1
a = 0.3
a = 0.5
5 – 81
4094A17

Fig. 21

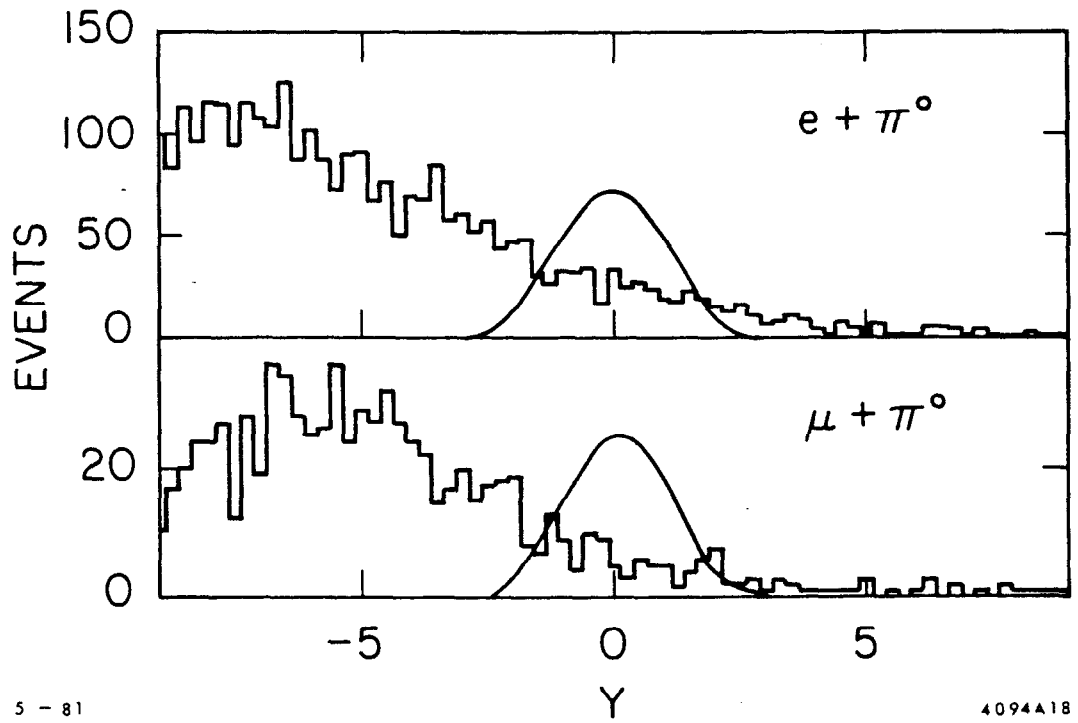

Fig. 22

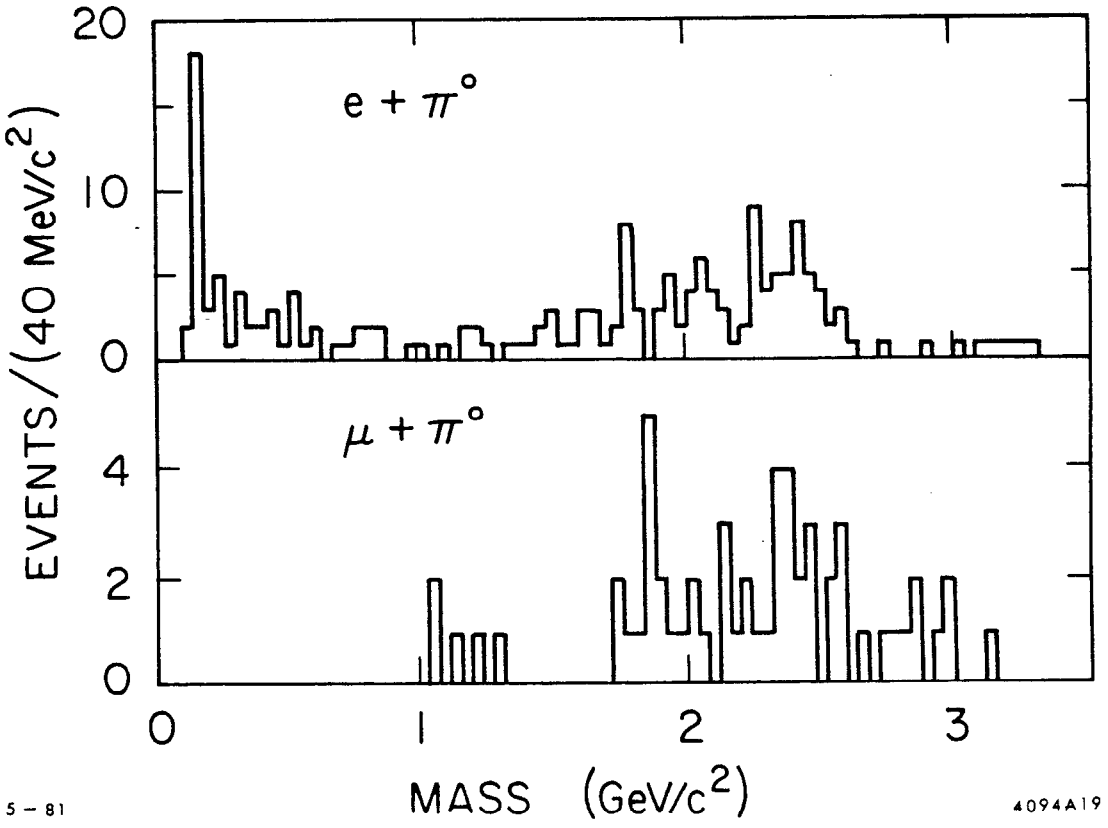

Fig. 23

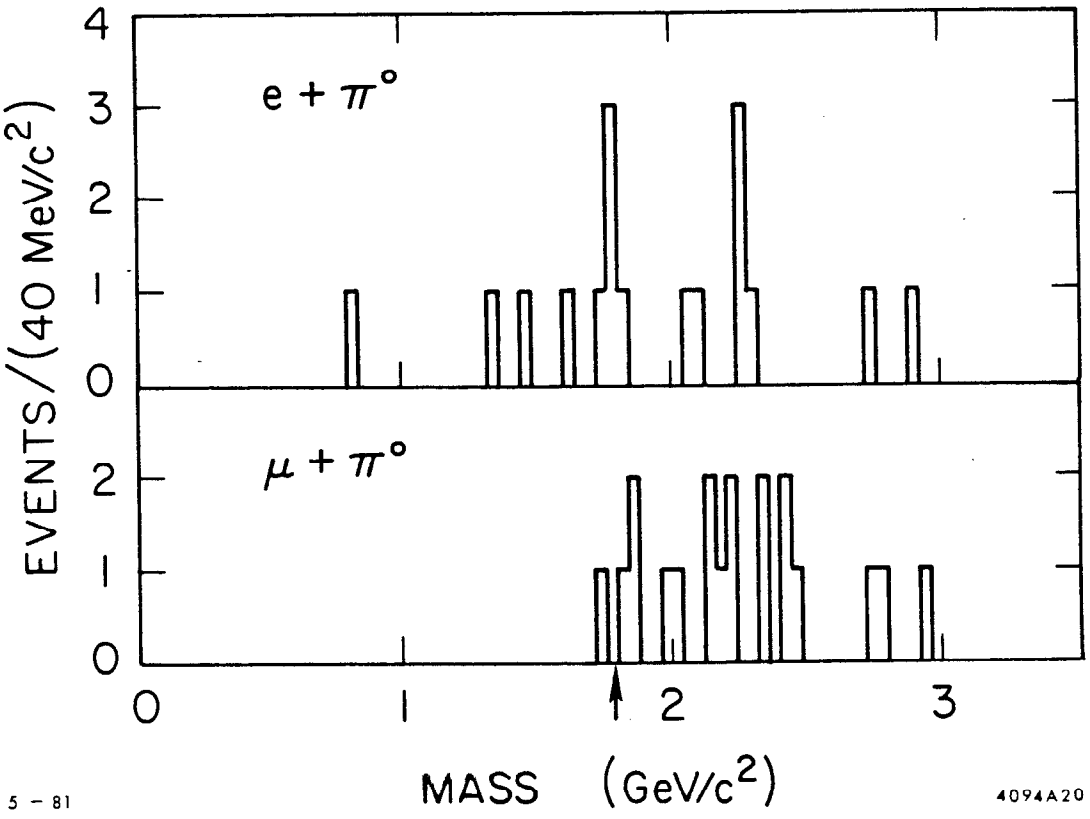

Fig. 24

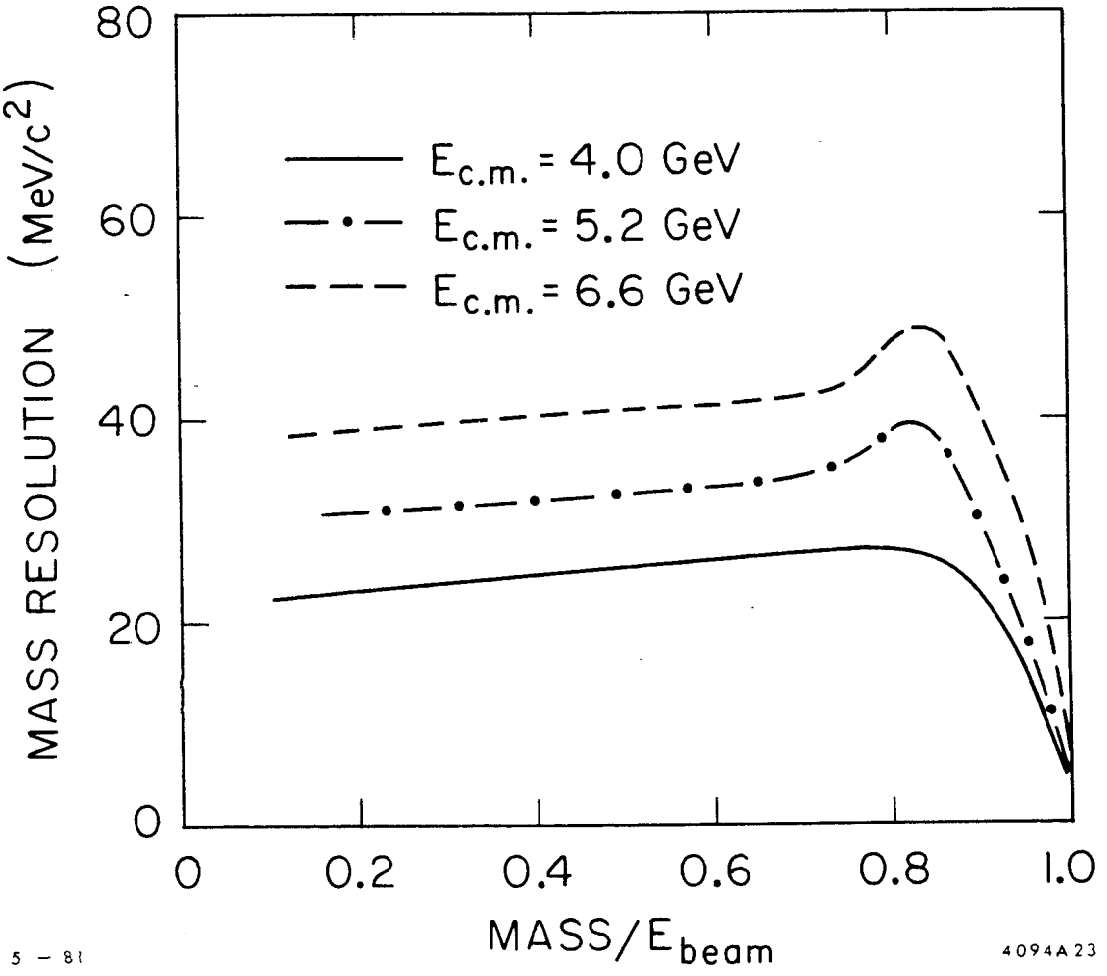
80
60
40
20
0
0
0.2
0.4
0.6
0.8
1.0
MASS RESOLUTION (MeV/c²)
MASS/E beam
E c.m. = 4.0 GeV
E c.m. = 5.2 GeV
E c.m. = 6.6 GeV
5 – 81
4094A23

Fig. 25

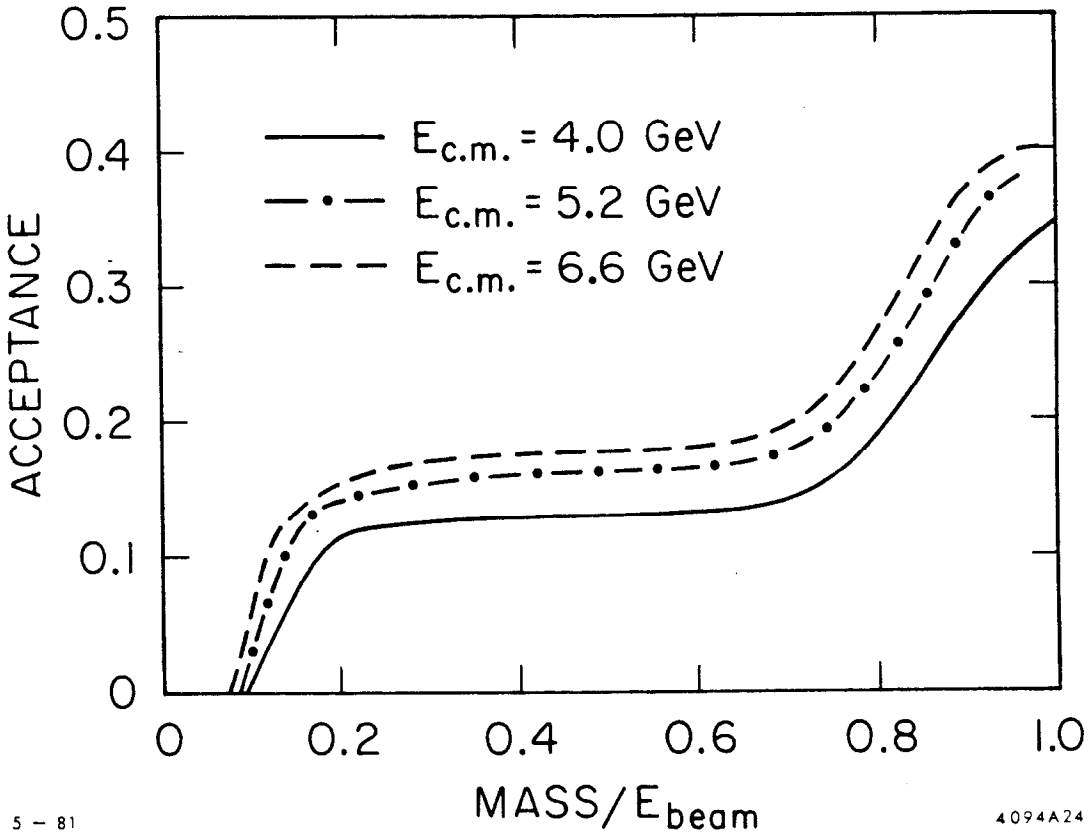
0.5
0.4
0.3
0.2
0.1
0
ACCEPTANCE
$E_{c.m.}$ = 4.0 GeV
$E_{c.m.}$ = 5.2 GeV
$E_{c.m.}$ = 6.6 GeV
0
0.2
0.4
0.6
0.8
1.0
MASS/E_{beam}
5 – 81
4094A24

Fig. 26

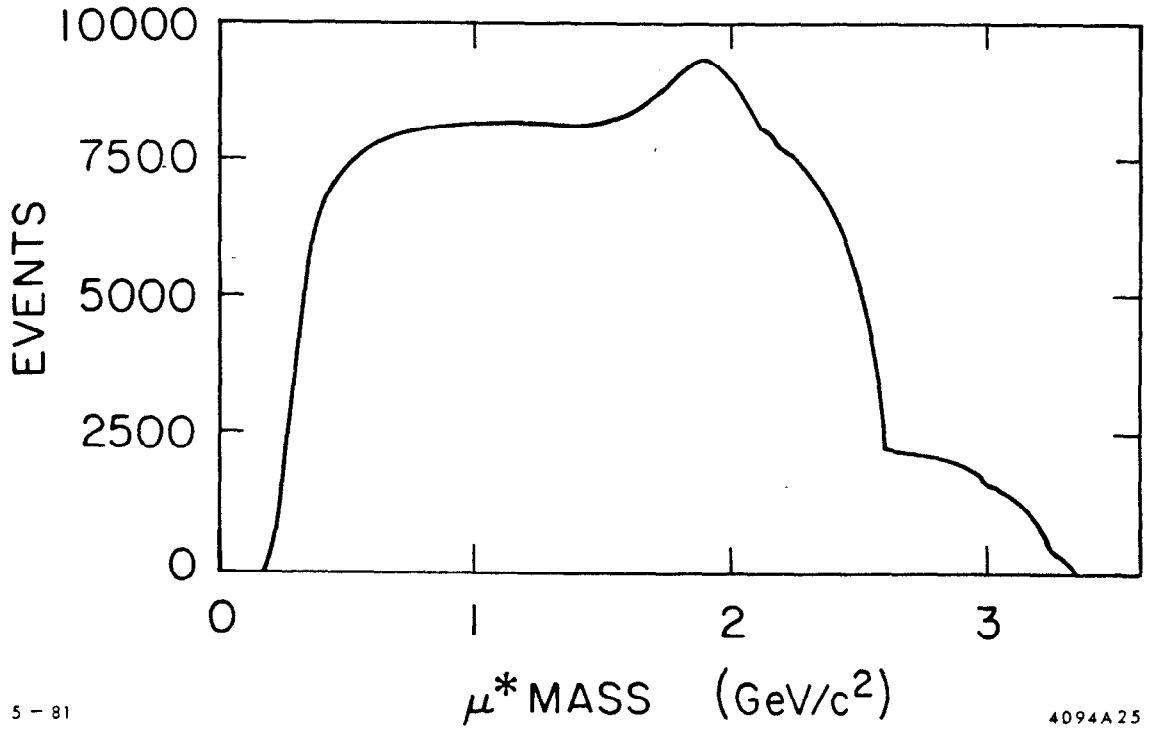

Fig. 27

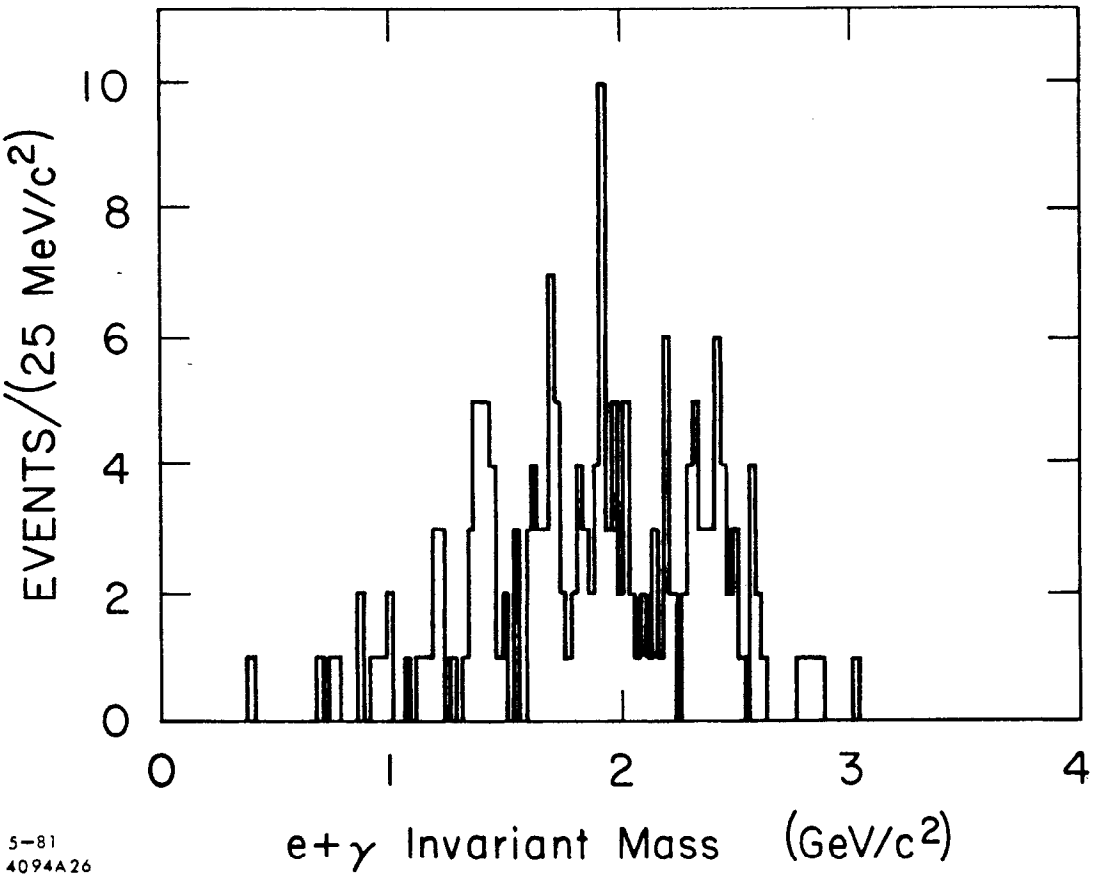
EVENTS/(25 MeV/c²)
0
2
4
6
8
10
0
1
2
3
4
e+γ Invariant Mass (GeV/c²)
5-81
4094A26

Fig. 28

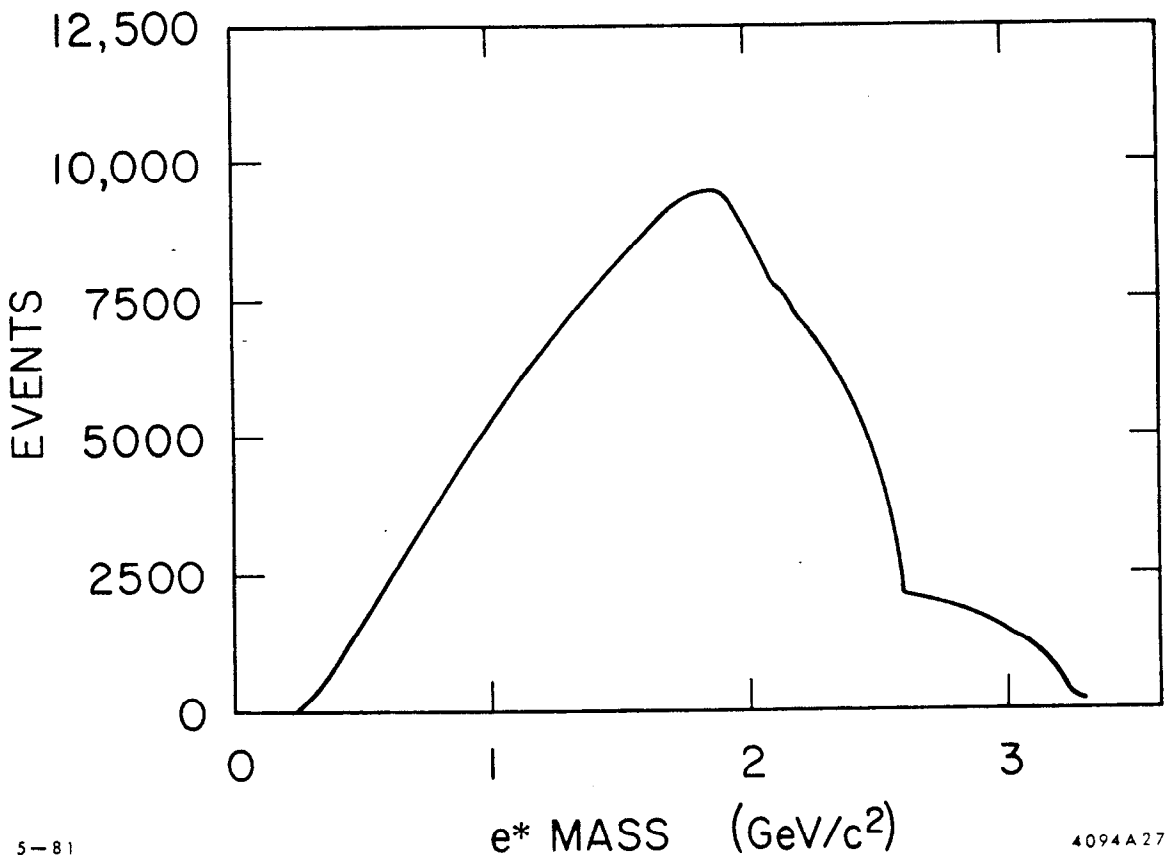
12,500
10,000
7500
5000
2500
0
EVENTS
0
1
2
3
e* MASS (GeV/c²)
5-81
4094A27

Fig. 29